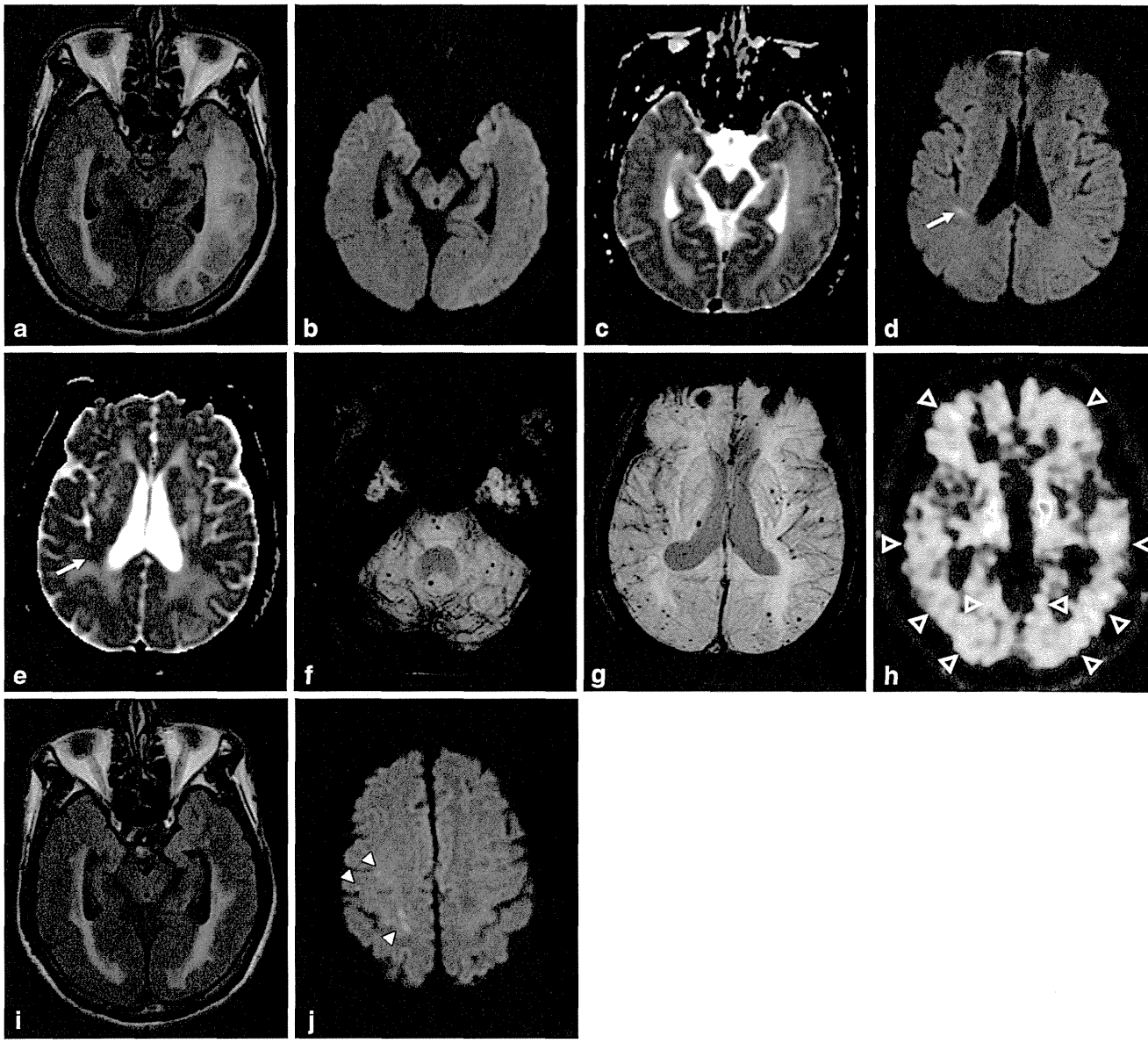

Fig. 2 CAA-related inflammation, MBs, and microinfarctions in a 72-year-old man. An axial FLAIR image (**a**) showed large confluent asymmetric hyperintense lesions, which involved not only the left dominant subcortical white matter but also the overlying left temporo-occipital cortices, with a mass effect. Low signal intensity on DWI (**b**) and increased diffusion on the ADC map (**c**) suggested vasogenic oedema. In addition to these white matter lesions, DWI (**d**) demonstrated a small right temporal hyperintense lesion (*arrow*) with corresponding decreased diffusion (*arrow*) on the ADC map (**e**) (*arrow*). This signal change indicated a relatively acute microinfarction. An axial 3D T2*-weighted image (**f**, **g**) revealed multiple MBs, which were distributed not only in the posterior dominant cortical-subcortical region but also in the left putamen, right thalamus, pons and cerebellum. A PiB-PET image (**h**) revealed the diffuse cortical accumulation, including the occipital lobes, higher than those of the cerebral white matter, which indicated the global PiB uptake (*open arrowheads*). These finding of MBs and PiB distribution suggested the coexistence of CAA and hypertensive arteriopathy. Two months after a course of intravenous steroid therapy, an improvement in the white matter lesions was identified on a FLAIR image (**i**). However, DWI (**j**) revealed new subcortical microinfarctions in the right frontal lobe (*arrowheads*)

CAA on the Boston criteria in the Table 3) [11]. Similar to the distribution of CAA pathology and CAA-related lobar ICHs, the distribution of CAA-related MBs appears to show a posterior cortical predominance (Figs. 1, 2 and 6) [18]. GRE sequences are the recommended method for MB detection due to the insensitivity of MB detection on CT and spin-echo sequences of MRI. Furthermore, considering the limitation of conventional T2* GRE sequences, which have underestimated MBs in 25 % of CAA patients, more sensitive sequences such as SWI and PRESTO sequences should be used to increase the detection rates of MBs (Fig. 1) [9]. It is notable that neuroimaging study has revealed lobar MBs in more than 20 % of patients with AD (Fig. 7), which may reflect advanced CAA in keeping with neuropathological findings [23].

Table 3 Classic and modified Boston criteria [11, 19]

	Classic Boston criteria	Modified Boston criteria
Definite CAA	Full post-mortem examination demonstrating: - Lobar, cortical or corticosubcortical haemorrhage - Severe CAA with vasculopathy - Absence of other diagnostic lesion	No modification
Probable CAA with supporting pathology	Clinical data and pathological tissue (evaluated) haematoma or cortical biopsy) demonstrating: - Lobar, cortical or corticosubcortical haemorrhage - Some degree of CAA in specimen - Absence of other diagnostic lesion	No modification
Probable CAA	Clinical data and MRI or CT demonstrating: - Multiple haemorrhages restricted to lobar, cortical or corticosubcortical regions (cerebellar haemorrhage allowed) - Age ≥55 - Absence of other cause of haemorrhage	Clinical data and MRI or CT demonstrating: - Multiple haemorrhages restricted to lobar, cortical or corticosubcortical regions (cerebellar haemorrhage allowed), or - Single lobar, cortical, or corticosubcortical haemorrhage and focal or disseminated superficial siderosis - Age ≥55 - Absence of other cause of haemorrhage or superficial siderosis
Possible CAA	Clinical data and MRI or CT demonstrating: - Single lobar, cortical or corticosubcortical haemorrhage - Age ≥55 - Absence of other cause of haemorrhage	Clinical data and MRI or CT demonstrating: - Single lobar, cortical or corticosubcortical haemorrhage, or - Focal or disseminated superficial siderosis - Age ≥55 - Absence of other cause of haemorrhage or superficial siderosis

Subarachnoid haemorrhage: a predictive finding of unfavourable outcomes?

Recently, CAA has been increasingly reported as a cause of SAHs in the elderly, especially those localised at the convexity of the brain (cSAH) [24, 25]. CAA-related cSAH may be due to direct extension of the cortical-subcortical haemorrhage into the subarachnoid or to primary SAH resulting from disruption of the leptomeningeal vessels by β-amyloid (Figs. 4 and 6) [8]. The clinical presentation of CAA-related cSAH is distinct because patients suffer from transient focal neurological deficits, including motor or sensory symptoms and seizures, rather than typical headaches [24, 25]. Such symptomatic cSAHs are mainly located within the central sulcus. Whether cSAH could be a warning sign of subsequent ICHs depends on the underlying disease. CAA-related cSAH often recurs, and a high rate of subsequent cerebrovascular disorders including infarctions and ICHs could contribute to unfavourable outcomes, including neurological disability and death in the elderly [25, 26].

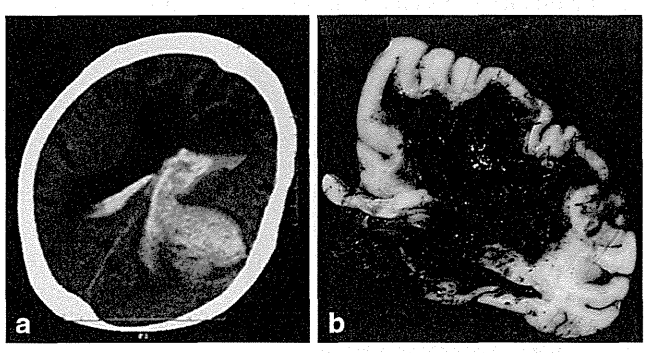

Fig. 3 Fetal CAA-related ICH with associated massive ventricular haemorrhage in a 92-year-old woman. A CT scan (**a**) revealed large left-sided parietal subcortical ICH extending into the left lateral ventricle, which caused hydrocephalic ventricular dilatation. A huge subcortical and intraventricular haematoma was identified on a macroscopic specimen at autopsy (**b**)

Unenhanced head CT has shown a slight, sometimes barely visible, sulcal hyperattenuation, most frequently depicted around the precentral gyrus [26]. Subsequent MRI scans confirmed the subarachnoid haemorrhage as a hyperintense area on FLAIR images (Fig. 6). In addition to this subarachnoid lesion, GRE sequences, especially SWI and PRESTO images, showed multiple lobar cortical-subcortical haemorrhagic lesions (macrohaemorrhages or MBs) (Fig. 6) [24, 25]. Considering the high prevalence of MBs and SS in CAA patients [24], these abnormal findings should be evaluated in the diagnosis of cSAH. It is also to be noted that CAA-related cSAH and SS can be present without other haemorrhagic lesions, including ICHs and MBs [19].

Superficial siderosis: a clinical entity distinct from the well-known classical SS

It is estimated that repeated cSAH leads to haemosiderin deposits in the subpial layers of the supratentorial brain [19].

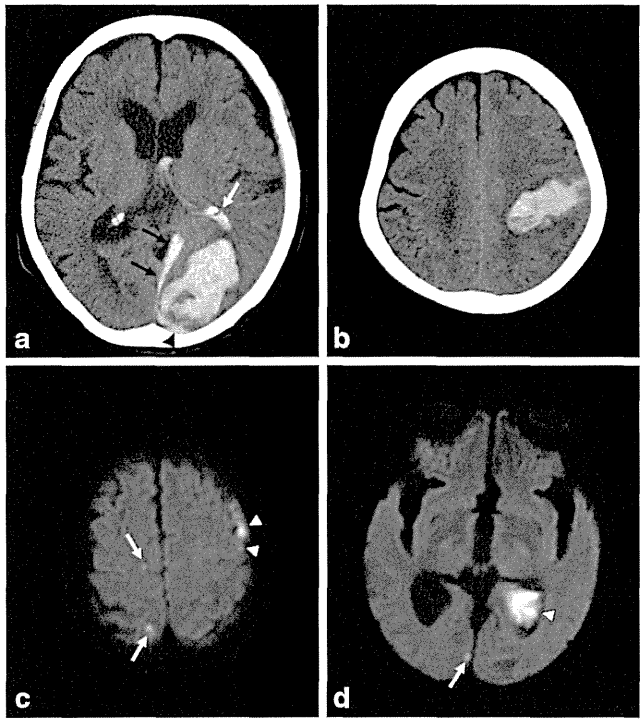

Fig. 4 Recurrent CAA-related ICHs associated with intraventricular, subdural and subarachnoid haemorrhages, and microinfarctions in an 87-year-old woman. A CT scan (**a**) showed left-sided occipital subcortical ICH extending into the left lateral ventricle (*white arrow*), and the subdural (*black arrows*) and subarachnoid space (*arrowhead*) around the occipital lobe. Seven months later, left-sided parietal subcortical ICH recurred and extended into the left ventricle. In addition to these haemorrhagic lesions, asymptomatic cortical microinfarctions (*arrows*) were identified on DWI 12 days after the first (**c**) and 13 days after recurrent ICH (**d**). *Arrowheads* indicated subdural, subarachnoid and intraventricular haemorrhages

In addition to other lobar haemorrhagic lesions, SS depicted predominantly in the supratentorial area has been increasingly recognised as one of the CAA-related abnormal findings [24]. A recent report has revealed that CAA-related SS as well as cSAH can be a warning sign of future intracranial haemorrhagic lesions [27].

Considering the marked difference of SS prevalence observed between CAA and non-CAA patients, the inclusion of SS in the modified Boston criteria may enhance their sensitivity for the diagnosis of CAA without a loss in specificity (Table 3) [19]. Furthermore, SS can be the important indicator of CAA in AD patients beyond the MBs or ICHs that are more readily recognised as being CAA-related haemorrhagic lesions (Fig. 7) [28].

CAA-related SS on GRE sequences showed the characteristic 'gyriform' pattern of a hypointense signal (Figs. 6 and 7). Generally, proton density and FLAIR images or unenhanced CT scans are used to identify acute SAHs and to distinguish them from chronic SS [27]. This abnormal signal intensity revealed a preference for the cerebral convexity and only exceptionally occurred in the infratentorial area [19]. This distribution explains why CAA-related SS may be associated with transient neurological manifestations and lacks the typical clinical presentation associated with the well-known SS, namely cerebellar and brainstem signs [19].

CAA-related inflammation—treatable form of a CAA-related disorder

In addition to haemorrhagic complications, a syndrome of perivascular inflammation and oedema has been recognised in the spectrum of presentations associated with CAA [29]. Pathologically, CAA-related inflammation reveals vascular amyloid deposition accompanied by perivascular, intramural and/or transmural inflammatory changes, with or without granuloma formation. The mechanism by which this immune response occurs is not well understood, although one possible factor is the increased frequency of the apolipoprotein E ε4/ε4 genotype [5, 29]. The clinical presentation of CAA-related inflammation typically manifests as headache, subacute cognitive decline and seizures [5, 29]. The apparent response of most patients to immunosuppressive therapy suggests that this disorder represents a treatable form of CAA, which highlights the importance of reaching this diagnosis in practice (Fig. 2).

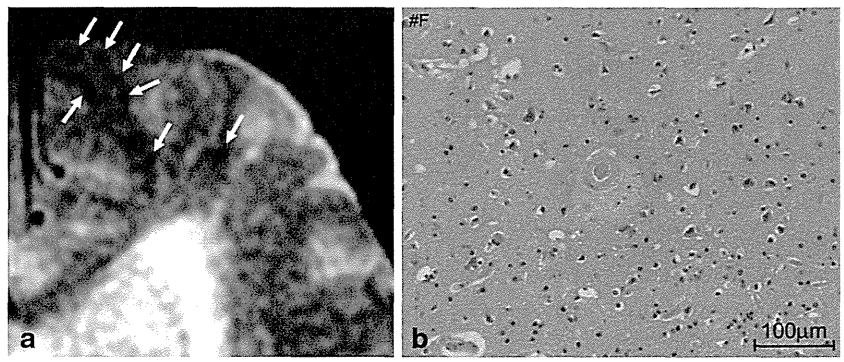

Fig. 5 Pathologically proved subcortical MBs in a 76-year-old man. An axial GRE T2*-weighted image (**a**) showed multiple cortical-subcortical hypointense foci suggestive of CAA-related MBs (*arrows*). A histopathological section corresponding to MBs (haematoxylin and eosin stain) (**b**) revealed amyloid deposits in the vessel walls with perivascular leakage of erythrocytes and plasma

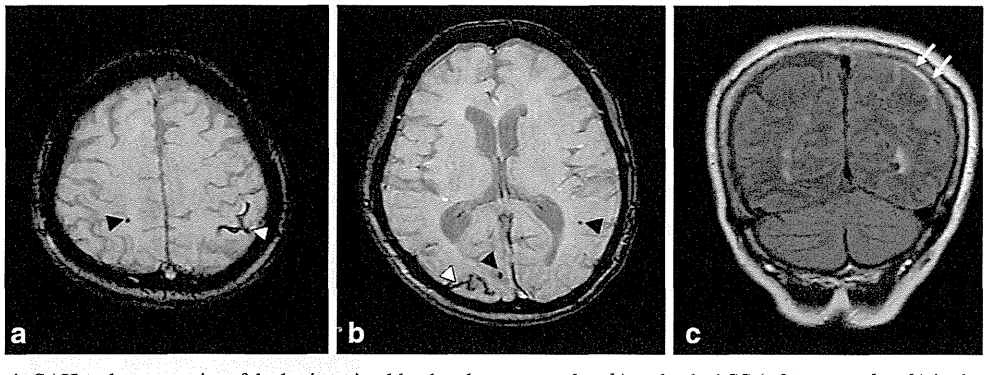

Fig. 6 Non-traumatic SAH at the convexity of the brain, microbleed and SS in a 72-year-old woman who was clinically diagnosed with AD. Axial 3D T2*-weighted images (**a**, **b**) showed bilateral subcortical MBs (*black arrowheads*) and sulcal SS (*white arrowheads*) in the posterior dominant distribution. Additionally, SAH along the left parietal sulci (*arrows*) was identified on a coronal FLAIR image (**c**)

However, CAA-related inflammation could also be not only a stable/progressive disorder but also a relapsing disorder, and the proportion crossing over from "improved" to "relapsing" disease may increase with longer follow-ups [5].

CAA-related inflammation is characterised by large confluent asymmetric white matter lesions of abnormal attenuation/intensity extending to the subcortical white matter and occasionally the overlying cortical grey matter with mass effect (Figs. 1 and 2). These lesions are depicted more clearly on MRI than on CT, especially on the FLAIR sequence, and involve one or more cortical territories, distributed almost equally across the frontal, parietal, temporal and occipital

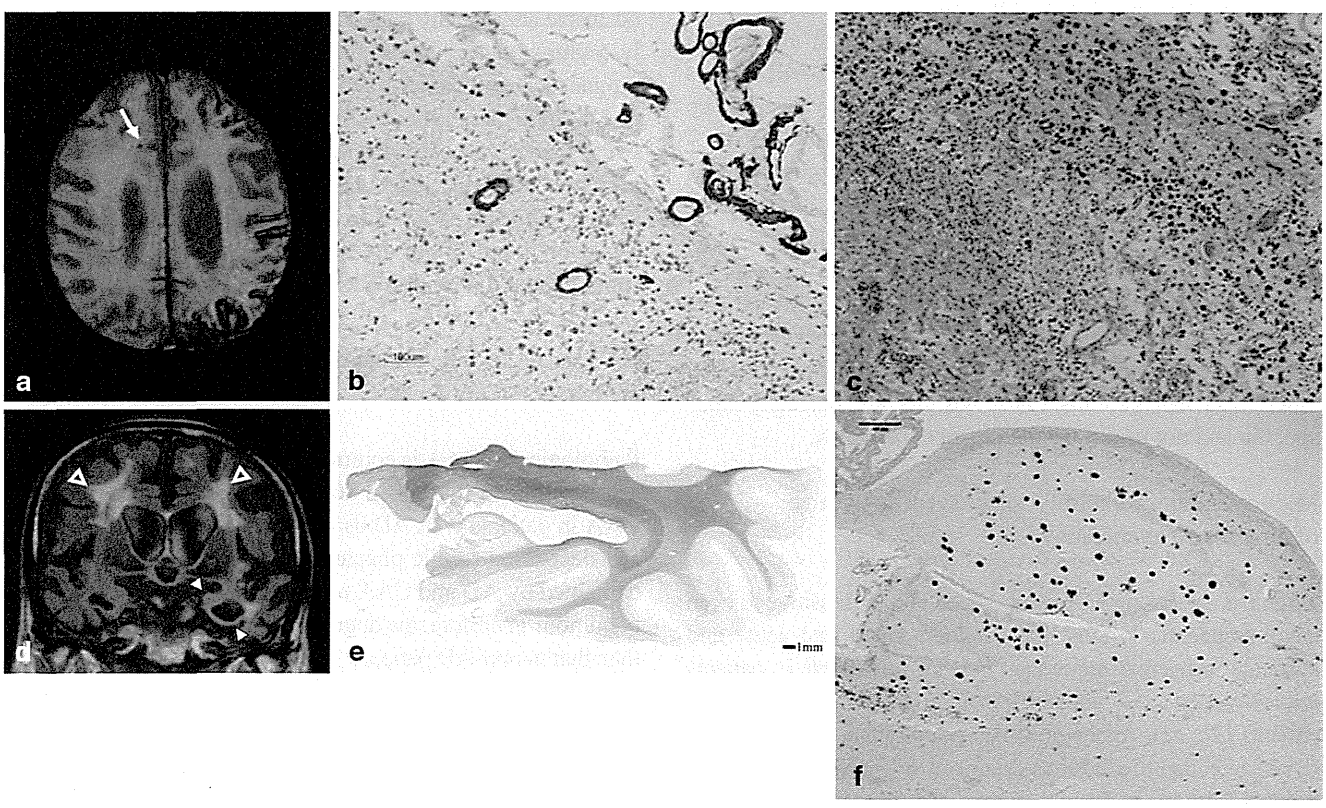

Fig. 7 CAA-related SS and MB in a 90-year-old man with pathologically proved AD. In addition to the right frontal subcortical MB (*arrow*), a 3D T2*-weighted image (**a**) demonstrated the typical gyriform low signals along the left cerebral sulci. Severe amyloid beta immunoreactive deposits were present in the leptomeningeal and cortical vessel walls of the parietal lobe (immunohistochemistry raised against monoclonal antibody Aβ 11–28) (**b**). The upper cortical layers were necrotic. Numerous haemosiderin-laden macrophages were present in the subarachnoid space and upper cortical layers (haematoxylin and eosin stain). These findings were consistent with superficial siderosis. A coronal FLAIR image (**d**) demonstrated left dominant atrophy of the amygdala and parahippocampal gyrus (*arrowheads*), and symmetric deep white matter hyperintensities (*open arrowheads*). A section of the left posterior hippocampus revealed atrophy of the hippocampus proper, subiculum and parahippocampal gyrus. Pallor of the subcortical white matter was evident (Klüver-Barrera stain) (**e**). There were numerous Aβ 11–28 immunoreactive senile plaques in the hippocampus (**f**)

lobes without evident preferential laterality [5]. DWI and ADC maps can add further information suggestive of vasogenic oedema (Fig. 2). Interestingly, the clinical and neuroimaging feature of this condition is similar to the vasogenic oedema of amyloid-related imaging abnormalities (ARIA) associated with amyloid-modifying therapy. A potential connection between CAA-related inflammation and immunotherapy-associated ARIA has been recently suggested by identification of anti-Aβ autoantibodies in the CSF of a patient with the spontaneously occurring syndrome [30].

Leukoaraiosis: a common but by no means specific finding of CAA

Leukoaraiosis is a radiological term which describes the abnormal imaging changes in the deep cerebral white matter. Pathological changes include demyelination, axon loss and mild gliosis. CAA-related impairments of perfusion due to amyloid in the overlying cortical small vessels probably cause the leukoaraiosis in CAA patients [3, 32]. Another possible mechanism of leukoaraiosis in CAA is as a result of the accumulation of silent ischaemic lesions [3].

Leukoaraiosis appears as diffuse or focal low attenuation on CT or hyperintensity on T2-weighted and FLAIR images on MRI, which is prevalent in the centrum semiovale and deep white matter with sparing of the subcortical U fibres (Figs. 7 and 8) [8]. In contrast to CAA-related inflammation, this finding is irreversible. As well as hypertensive arteriopathy, CAA-related leukoaraiosis preferentially affects the same periventricular regions; however, some studies suggest the posterior dominant white matter involvement in CAA patients [3, 32] (Fig. 8). Although advanced CAA is associated with a large burden of white matter lesions compared with healthy elders and AD patients, these lesions are basically non-specific and not useful for the diagnosis of CAA.

Microinfarction: a clinically silent event suggestive of progressive arteriopathy

Recent studies using MR DWI, which is very sensitive to even small ischaemic lesions, have demonstrated that acute and subacute ischaemic infarctions are not infrequent in patients with advanced CAA, and occur in approximately 15 % of these patients [31, 32]. Analyses of autopsied brains with advanced CAA have identified lesions described as perivascular scars or small infarctions at frequencies ranging from 37 % to nearly 100 % [32]. These pathologically observed infarctions are frequently multiple and located in the cortical ribbon or underlying subcortical white matter. Impaired cerebral blood flow regulation due to CAA-related occlusive arteriopathy may be related to these ischaemic changes [32]. Their presence was shown to be unrelated to conventional vascular risk factors such as hypertension, diabetes and coronary artery disease, and was instead associated with the severity of white matter lesions and lobar MBs, which suggests that they are due to CAA-related occlusive arteriopathy [31]. These lesions appear to be clinically asymptomatic; however, the therapeutic implications and prognostic significance of these findings require further study.

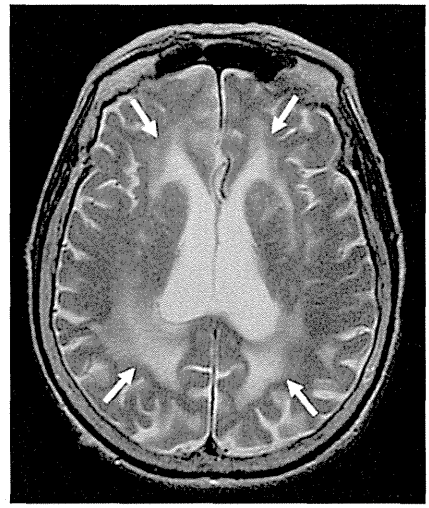

Fig. 8 Leukoaraiosis in an 87-year-old woman with pathologically proved CAA and AD. Axial T2-weighted images showed bilateral hyperintensities (*arrows*), which involved the posterior dominant periventricular and deep white matters

On MRI, these lesions are located mainly in the subcortical white matter and cortical grey matter away from the site of previous ICHs [31, 32]. They may also be located in the cerebellum. Acute lesions were identified as small and mostly ovoid or round bright areas on DWI sequences and corresponding dark areas on ADC maps (Figs. 2 and 4).

CAA and AD—representation of two sides of a single condition: Aβ amyloidosis

Pathologically, CAA is commonly found in AD (Fig. 7), with a prevalence of more than 80 % [2]. The high prevalence of CAA in patients with AD as well as of cerebral parenchymal Aβ deposition (senile plaques) in patients with CAA can be explained by AD and CAA representing two sides of a single condition. Therefore, the degree of CAA in AD is more severe than that in non-AD patients. It is noteworthy that the presence of CAA may have a significant impact on the clinical course of AD. The coexistence of CAA with AD has been reported to impair cognitive performance more significantly than AD alone, even after adjustments for age, neurofibrillary tangle and amyloid plaque number, and infarctions [33].

Differential diagnosis

A single large cortical-subcortical ICH presenting with an acute neurological deficit is not entirely specific for a

diagnosis of CAA. Various disorders, including hypertensive arteriopathy, haemorrhagic tumours, vascular malformation, trauma, bleeding diatheses and illicit drug use such as amphetamines and cocaine, can cause cortical-subcortical ICHs [8]. Notably, infectious aneurysm can cause not only subcortical ICH but also SAH and MBs like signal change. In the diagnosis of subcortical haemorrhagic lesions, it is sometimes difficult to narrow the differential diagnosis because of its non-specific nature. Therefore, to evaluate other abnormal findings suggestive of CAA (i.e. MBs and SS) is mandatory for the precise diagnosis. Gadolinium enhancement and MR angiogram are also useful to evaluate the tumorous and vascular lesions, respectively.

The hypertensive arteriopathy as well as CAA is the most common cause of MBs. Less common causes include diffuse axonal injury, cerebral fat embolism, cerebral autosomal dominant arteriopathy with subcortical infarcts and leukoencephalopathy (CADASIL), multiple cavernous malformations, vasculitis, radiation vasculopathy and so on. To understand the distinctive cortical-subcortical distributions that generally spare the basal ganglia and brainstem is important for the diagnosis of CAA. To check the other imaging findings such as restricted diffusion of axonal injury, multiple white matter lesions—especially in the temporal pole of CADASIL—and vascular lesions of vasculitis, are also contributory to diagnosis.

Convexal SAH and SS are important subtypes of nonaneurysmal subarachnoid bleeding and its sequela with diverse aetiologies. Although CAA is frequent in patients older than 60 years, a reversible vasoconstriction syndrome appears to be a common cause of cSAH in younger patients [24]. Other than those above, cSAH carries a broad differential diagnosis, including head trauma, posterior reversible encephalopathy syndrome (PRES), dural sinus and cortical venous thrombosis, vascular malformation, vasculitis and anticoagulation [34]. Parenchymal abnormalities, including cerebral contusions and subcortical white matter lesions, are useful to diagnose head trauma and PRES. Additionally, to check the vascular lesion, especially the dural sinus and cortical vein, is crucial for the diagnosis of thromboses and malformations.

Because various pathological conditions, including PRES, infections (e.g. progressive multifocal leukoencephalopathy), acute disseminated encephalomyelitis and malignancies (e.g. primary CNS lymphoma and gliomatosis cerebri), can manifest as multiple white matter lesions [35], the essential step in the diagnosis of CAA-related inflammation is the recognition of CAA. In other words, GRE sequences including SWI and PRESTO images, which enable recognition of CAA-related MBs and SS, are fundamental in diagnosing CAA-related inflammation without invasive brain biopsy (Fig. 2) [5]. Considering that a part of the CAA-related inflammation may manifest as non-haemorrhagic white matter lesions, PiB-PET should be regarded as a supplementary diagnostic technique.

In addition to above-described imaging findings, it is also necessary to evaluate the medical history, physical examination findings and laboratory results to differentiate CAA from its mimickers. For example, typical medical history such as the elevated blood pressure and chemotherapy is usually associated with PRES and helps to clarify the diagnosis.

Conclusions

In the various types of CAA-related abnormal findings, haemorrhagic lesions, especially lobar restricted ICHs and MBs, cSAH and supratentorial SS, in the elderly can be crucial imaging findings of CAA. Furthermore, CAA can reveal other imaging findings including CAA-related inflammation and microinfarction. Radiologists should understand that MRI, especially GRE and FLAIR sequences, can non-invasively provide clues for the diagnosis of CAA-related disorders. CAA-related imaging findings are not always specific; therefore, it is necessary to combine with other CAA-related imaging findings for the diagnosis. Amyloid PET can be an important clue to differentiate CAA from other pathological conditions, such as hypertension and bleeding diatheses, which cause similar and mistakable haemorrhagic imaging findings.

Acknowledgments We have received the support for the English proofreading from a Grant-in-Aid for Scientific Research (Kakenhi C) (24591785, K.S. and 23500435, M.T.), Research on Measures for Intractable Diseases (M.T.) (H24-nanchi-ippan-063, Nanchi-ippan-013) and the Comprehensive Brain Science Network (S.M., M.T.).

References

1. Attems J, Lintner F, Jellinger KA (2004) Amyloid beta peptide 1–42 highly correlates with capillary cerebral amyloid angiopathy and Alzheimer disease pathology. Acta Neuropathol 107:283–291
2. Yamada M, Tsukagoshi H, Otomo E, Hayakawa M (1987) Cerebral amyloid angiopathy in the aged. J Neurol 234:371–376
3. Charidimou A, Gang Q, Werring DJ (2012) Sporadic cerebral amyloid angiopathy revisited: recent insights into pathophysiology and clinical spectrum. J Neurol Neurosurg Psychiatry 83:124–137
4. Biffi A, Halpin A, Towfighi A, Gilson A, Busl K, Rost N, Smith EE, Greenberg MS, Rosand J, Viswanathan A (2010) Aspirin and recurrent intracerebral hemorrhage in cerebral amyloid angiopathy. Neurology 75:693–698
5. Kinnecom C, Lev MH, Wendell L, Smith EE, Rosand J, Frosch MP, Greenberg SM (2007) Course of cerebral amyloid angiopathy-related inflammation. Neurology 68:1411–1416
6. McCarron MO, Nicoll JA (2004) Cerebral amyloid angiopathy and thrombolysis-related intracerebral haemorrhage. Lancet Neurol 3: 484–492

7. Greenberg SM, Finklestein SP, Schaefer PW (1996) Petechial hemorrhages accompanying lobar hemorrhage: detection by gradient-echo MRI. Neurology 46:1751–1754
8. Chao CP, Kotsenas AL, Broderick DF (2006) Cerebral amyloid angiopathy: CT and MR imaging findings. Radiographics 26:1517–1531
9. Charidimou A, Krishnan A, Werring DJ, Rolf Jäger H (2013) Cerebral microbleeds: a guide to detection and clinical relevance in different disease settings. Neuroradiology 55:655–674
10. Sakurai K, Kawaguchi T, Kawai T, Ogino H, Hara M, Okita K, Yamawaki T, Shibamoto Y (2010) Usefulness of 3D-PRESTO imaging in evaluating putaminal abnormality in parkinsonian variant of multiple system atrophy. Neuroradiology 52:809–814
11. Knudsen KA, Rosand J, Karluk D, Greenberg SM (2001) Clinical diagnosis of cerebral amyloid angiopathy: validation of the Boston criteria. Neurology 56:537–539
12. Klunk WE, Engler H, Nordberg A, Wang Y, Blomqvist G, Holt DP, Bergström M, Savitcheva I, Huang GF, Estrada S, Ausén B, Debnath ML, Barletta J, Price JC, Sandell J, Lopresti BJ, Wall A, Koivisto P, Antoni G, Mathis CA, Långström B (2004) Imaging brain amyloid in Alzheimer's disease with Pittsburgh Compound-B. Ann Neurol 55:306–319
13. Greenberg SM, Grabowski T, Gurol ME, Skehan ME, Nandigam RN, Becker JA, Garcia-Alloza M, Prada C, Frosch MP, Rosand J, Viswanathan A, Smith EE, Johnson KA (2008) Detection of isolated cerebrovascular beta-amyloid with Pittsburgh compound B. Ann Neurol 64:587–591
14. Fazekas F, Kleinert R, Roob G, Kleinert G, Kapeller P, Schmidt R, Hartung HP (1999) Histopathologic analysis of foci of signal loss on gradient-echo T2*-weighted MR images in patients with spontaneous intracerebral hemorrhage: evidence of microangiopathy-related microbleeds. AJNR Am J Neuroradiol 20:637–642
15. Vinters HV (1987) Cerebral amyloid angiopathy. A critical review. Stroke 18:311–324
16. Arima H, Tzourio C, Anderson C, Woodward M, Bousser MG, MacMahon S, Neal B, Chalmers J, PROGRESS Collaborative Group (2010) Effects of perindopril-based lowering of blood pressure on intracerebral hemorrhage related to amyloid angiopathy: the PROGRESS trial. Stroke 41:394–396
17. O'Donnell HC, Rosand J, Knudsen KA, Furie KL, Segal AZ, Chiu RI, Ikeda D, Greenberg SM (2000) Apolipoprotein E genotype and the risk of recurrent lobar intracerebral hemorrhage. N Engl J Med 342:240–245
18. Rosand J, Muzikansky A, Kumar A, Wisco JJ, Smith EE, Betensky RA, Greenberg SM (2005) Spatial clustering of hemorrhages in probable cerebral amyloid angiopathy. Ann Neurol 58:459–462
19. Linn J, Halpin A, Demaerel P, Ruhland J, Giese AD, Dichgans M, van Buchem MA, Bruckmann H, Greenberg SM (2010) Prevalence of superficial siderosis in patients with cerebral amyloid angiopathy. Neurology 74:1346–1350
20. Schrag M, McAuley G, Pomakian J, Jiffry A, Tung S, Mueller C, Vinters HV, Haacke EM, Holshouser B, Kido D, Kirsch WM (2010) Correlation of hypointensities in susceptibility-weighted images to tissue histology in dementia patients with cerebral amyloid angiopathy: a postmortem MRI study. Acta Neuropathol 119:291–302
21. Werring DJ, Frazer DW, Coward LJ, Losseff NA, Watt H, Cipolotti L, Brown MM, Jäger HR (2004) Cognitive dysfunction in patients with cerebral microbleeds on T2*-weighted gradient-echo MRI. Brain 127:2265–2275
22. Greenberg SM, Eng JA, Ning M, Smith EE, Rosand J (2004) Hemorrhage burden predicts recurrent intracerebral hemorrhage after lobar hemorrhage. Stroke 35:1415–1420
23. Cordonnier C, van der Flier WM (2011) Brain microbleeds and Alzheimer's disease: innocent observation or key player? Brain 134:335–344
24. Kumar S, Goddeau RP Jr, Selim MH, Thomas A, Schlaug G, Alhazzani A, Searls DE, Caplan LR (2010) Atraumatic convexal subarachnoid hemorrhage: clinical presentation, imaging patterns, and etiologies. Neurology 74:893–899
25. Beitzke M, Gattringer T, Enzinger C, Wagner G, Niederkorn K, Fazekas F (2011) Clinical presentation, etiology, and long-term prognosis in patients with nontraumatic convexal subarachnoid hemorrhage. Stroke 42:3055–3060
26. Raposo N, Viguier A, Cuvinciuc V, Calviere L, Cognard C, Bonneville F, Larrue V (2011) Cortical subarachnoid haemorrhage in the elderly: a recurrent event probably related to cerebral amyloid angiopathy. Eur J Neurol 18:597–603
27. Linn J, Wollenweber FA, Lummel N, Bochmann K, Pfefferkorn T, Gschwendtner A, Bruckmann H, Dichgans M, Opherk C (2013) Superficial siderosis is a warning sign for future intracranial hemorrhage. J Neurol 260:176–181
28. Feldman HH, Maia LF, Mackenzie IR, Forster BB, Martzke J, Woolfenden A (2008) Superficial siderosis: a potential diagnostic marker of cerebral amyloid angiopathy in Alzheimer disease. Stroke 39:2894–2897
29. Eng JA, Frosch MP, Choi K, Rebeck GW, Greenberg SM (2004) Clinical manifestations of cerebral amyloid angiopathy-related inflammation. Ann Neurol 55:250–256
30. DiFrancesco JC, Brioschi M, Brighina L, Ruffmann C, Saracchi E, Costantino G, Galimberti G, Conti E, Curtò NA, Marzorati L, Remida P, Tagliavini F, Savoiardo M, Ferrarese C (2011) Anti-Aβ autoantibodies in the CSF of a patient with CAA-related inflammation: a case report. Neurology 76:842–844
31. Kimberly WT, Gilson A, Rost NS, Rosand J, Viswanathan A, Smith EE, Greenberg SM (2009) Silent ischemic infarcts are associated with hemorrhage burden in cerebral amyloid angiopathy. Neurology 72:1230–1235
32. Viswanathan A, Greenberg SM (2011) Cerebral amyloid angiopathy in the elderly. Ann Neurol 70:871–880
33. Pfeifer LA, White LR, Ross GW, Petrovitch H, Launer LJ (2002) Cerebral amyloid angiopathy and cognitive function: the HAAS autopsy study. Neurology 58:1629–1634
34. Spitzer C, Mull M, Rohde V, Kosinski CM (2005) Non-traumatic cortical subarachnoid haemorrhage: diagnostic work-up and aetiological background. Neuroradiology 47:525–531
35. Chung KK, Anderson NE, Hutchinson D, Synek B, Barber PA (2011) Cerebral amyloid angiopathy related inflammation: three case reports and a review. J Neurol Neurosurg Psychiatry 82:20–26

PLOS ONE

The Homologous Carboxyl-Terminal Domains of Microtubule-Associated Protein 2 and TAU Induce Neuronal Dysfunction and Have Differential Fates in the Evolution of Neurofibrillary Tangles

Ce Xie[1], Tomohiro Miyasaka[1]*, Satomi Yoshimura[1], Hiroyuki Hatsuta[3], Sawako Yoshina[2], Eriko Kage-Nakadai[2], Shohei Mitani[2], Shigeo Murayama[3], Yasuo Ihara[1]

1 Department of Neuropathology, Faculty of Life and Medical Sciences, Doshisha University, Kyotanabe-shi, Kyoto, Japan, **2** Department of Physiology, Tokyo Women's Medical University School of Medicine, Shinjuku-ku, Tokyo, Japan, **3** Department of Neuropathology, Tokyo Metropolitan Institute of Gerontology, Itabashi-ku, Tokyo, Japan

Abstract

Microtubule-associated protein 2 (MAP2) and Tau are abundant neuronal microtubule-associated proteins. Both proteins have highly homologous carboxyl-terminal sequences that function as microtubule-binding domains. Whereas Tau is widely accepted as a pathoetiological factor in human tauopathies, including Alzheimer's disease (AD), it is not known whether there is a relationship between MAP2 and tauopathy. To better understand the pathological roles of MAP2 and Tau, we compared their behaviors in transgenic *Caenorhabditis elegans* in which MAP2 or Tau was expressed pan-neuronally. Both MAP2 and Tau elicited severe neuronal dysfunction and neuritic abnormalities, despite the absence of detergent-insoluble aggregates in worm neurons. Biochemical analysis revealed that the expressed MAP2 or Tau in worms was highly phosphorylated and did not bind to microtubules. Newly raised antibodies to MAP2 that effectively distinguished between the highly homologous carboxyl-terminal sequences of MAP2 and Tau showed that MAP2 was not involved in the growth process of neurofibrillary tangles in the AD brain. These results indicate that Tau and MAP2 have different fates in the inclusion formation and raise the possibility that MAP2 plays a significant role in neurotoxicity in the AD brain despite the absence of MAP2-aggregates.

Citation: Xie C, Miyasaka T, Yoshimura S, Hatsuta H, Yoshina S, et al. (2014) The Homologous Carboxyl-Terminal Domains of Microtubule-Associated Protein 2 and TAU Induce Neuronal Dysfunction and Have Differential Fates in the Evolution of Neurofibrillary Tangles. PLoS ONE 9(2): e89796. doi:10.1371/journal.pone.0089796

Editor: Emmanuel Planel, Centre Hospitalier de l'Université Laval, Canada

Received July 29, 2013; **Accepted** January 25, 2014; **Published** February 25, 2014

Funding: This work was supported in part by a Grant-in-Aid for Scientific Research (KAKENHI; Grant-in-Aid for Young Scientists (B); 20700324; T.M. and 24700368; C.X. and Grant-in-Aid for Challenging Exploratory Research; 22650074; T.M.) and by Core Research for Evolutional Science and Technology (CREST; T.M., C.X., and Y.I.), Japan Science and Technology Agency (JST). The funders had no role in study design, data collection and analysis, decision to publish, or preparation of the manuscript.

Competing Interests: The authors have declared that no competing interests exist.

* E-mail: tomiyasa@mail.doshisha.ac.jp

Introduction

Intracellular neurofibrillary tangles (NFTs) are the pathological hallmark of Alzheimer's disease (AD) and other tauopathies, including frontotemporal lobar degeneration, frontotemporal dementia and parkinsonism linked to chromosome 17 (FTDP-17), progressive supranuclear palsy, and corticobasal degeneration [1]. Tau is the principal component of NFTs [2]. Previous studies have indicated that the carboxyl-terminal half of Tau, which includes microtubule-binding domains (MTBDs), makes up the framework of NFTs [3,4]. By linkage analysis of FTDP-17, more than 30 missense mutations have been found in the exons and introns of the Tau gene. Interestingly, these mutations are almost all localized in or near MTBDs at the carboxyl-terminal region of Tau [1,5]. These observations strongly suggest an important relationship between the carboxyl-terminal region of Tau and the pathogenesis of tauopathies, although some reports have shown that the amino-terminal region of Tau contributes to its toxicity [6–8]. Notably, none of the reports has included a direct comparison in the same animal model system to identify the region responsible for Tau neurotoxicity.

Microtubule-associated protein 2 (MAP2) and Tau differ notably in their subcellular localization within neurons: whereas Tau is distributed abundantly in the axonal compartment, MAP2 is found exclusively in the somatodendritic compartment [9,10]. Both proteins have the homologous carboxyl-terminal sequences containing the MTBDs and distinct amino-terminal regions (projection domain). The MTBDs comprise three or four imperfect repeats of 31 amino acids in Tau (3R-Tau or 4R-Tau) and typically three repeats in MAP2 [11]. The common physiological role of MAP2 and Tau is considered to be the stabilization of microtubules, which may help maintain neuronal morphology [12,13]. MAP2 and Tau share highly homologous carboxyl-terminal sequences, but current information about the relationship between MAP2 and tauopathies is far from convincing.

Current data on the expression of human Tau in animal nervous systems have provided a key for better understanding how

tauopathies occur. Tauopathy models have been established using mice, nematodes, flies, and fish. *Caenorhabditis elegans* (*C.elegans*), which has a nervous system comprising 302 neurons, is a useful tool for the study of human neurodegenerative diseases [14–18]. To investigate the pathological role of Tau, in particular its carboxyl-terminal regions, which are highly homologous with those of MAP2, we produced transgenic worm models and subjected them to behavioral, biochemical, and morphological analyses. In addition, we raised new site-specific antibodies to MAP2 carboxyl-terminal sequences that do not cross-react with Tau. We used these antibodies to investigate the involvement of the homologous carboxyl-terminal regions of Tau and MAP2 in NFT formation in AD brains.

Materials and Methods

Ethics statement

Paraffin-embedded human brain sections and frozen autopsy brain tissues were obtained from the The Brain Bank for Aging Research, Tokyo Metropolitan Institute of Gerontology, Japan (URL: http://www.mci.gr.jp/BrainBank/index.cgi). This present study was approved by the ethics committee at Doshisha University and the institute (TMIG).

Plasmid construction

Human Tau and MAP2 cDNAs were amplified and cloned into *Not*I- and *Bgl*II-digested sites of the pFX vector. The Tau fragments and Tau/MAP2 chimeras were generated by polymerase chain reaction (PCR) and subcloned into the pFX vector. All constructs were under the control of the *unc-119* promoter for pan-neuronal expression, as described previously [19]. Plasmids were verified by DNA sequencing.

C. elegans strains

C. elegans strains were cultured under the conditions described previously [20]. Bristol strain N2 was used as the wild type. Transgenic lines of *C. elegans* were generated as described previously [18,21,22]. Briefly, constructs were injected into N2 strains with the marker Pges-1:: EGFP, which creates green fluorescence in the gut. Stable lines were generated by UV irradiation (300 J/m^2). Integrated lines were backcrossed to N2 twice before use.

To analyze the phenotype for uncoordinated movement (Unc), 20 young adult nematodes were placed on a fresh NGM plate to lay eggs at 20°C for 2 hours, and the adults were removed. Synchronized eggs were cultured at 20°C for 3 days until adults appeared. Twenty new young adult worms per line were transferred individually to new 3.5-cm plates, and Unc was analyzed immediately by multiple researchers under a blind method. The experiments were performed independently at least three times, and at least 60 worms were examined per line. Worms for each line were placed in the SDS sample buffer (0.08 M Tris HCl, 2% SDS, 10% glycerol, 1% 2-mercaptoethanol, pH 6.8), and the mixture was sonicated immediately. The combined lysate of 10 worms per line was subjected to western blotting. The transgenic lines for MAP2c fragments were analyzed without integration. Briefly, young adult worms that showed green fluorescence in gut were picked up and the Unc phenotype was analyzed under the blind method described above. The experiments were performed independently for three times and total thirty animals were analyzed per line.

Protein extraction and microtubule-binding assay

Four-day-old adult nematodes (tmIs390 for Tau; tmIs849 for MAP2) were harvested in M9 buffer (22 mM KH_2PO_4, 22 mM Na_2HPO_4, 85 mM NaCl, and 1 mM $MgSO_4$) and sonicated in Tris-saline buffer (TS; 50 mM Tris and 150 mM NaCl, pH 7.6) containing protease inhibitors (Roche) and phosphatase inhibitors (1 mM Na_3VO_4, 1 mM NaF, 1 μM okadaic acid, and 1 mM β-glycerophosphate). The homogenate was centrifuged at 120,000× *g* for 15 minutes at 2°C. The supernatant was adjusted to a final concentration of 0.5 M NaCl and 2% 2-mercaptoethanol, and was heated to 100°C for 7 minutes. Aggregated proteins and debris were removed by centrifugation at 20,000× *g* for 15 minutes at 2°C. The supernatant was adjusted to 50% ammonium sulfate, kept on ice for 15 minutes, and then centrifuged at 20,000× *g* for 15 minutes at 2°C. The pellet was resuspended and subjected to Lambda protein phosphatase (New England BioLabs, Inc.) treatment for 30 minutes at 30°C. The proteins were purified by repeating the above step of heating and ammonium sulfate precipitation as described above. For the microtubule-binding assay, 4-day-old adult nematodes (tmIs388, mock; tmIs390, Tau transgenic worm; tmIs849, MAP2c transgenic worm) were harvested and homogenized immediately in 0.1 M MES (pH 6.8), 1 mM EGTA, 1 mM $MgSO_4$, 2 mM DTT, and 0.5% Triton X-100 containing protease and phosphatase inhibitors at room temperature [23]. The homogenate was centrifuged at 120,000× *g* for 20 minutes at 20°C. The supernatant and pellet were saved separately and subjected to western blotting.

Preparation of human brain fractions

The frozen autopsy brain tissues from normal control and AD patients were at Braak stage I and Braak stage VI, respectively [24]. Human autopsy tissues from the temporal cortex were sequentially solubilized with TS, followed by TS containing 1% TritonX-100, 1% Sarkosyl, and 1% SDS, as described previously [25]. The Sarkosyl-insoluble, SDS-soluble fractions were subjected to SDS-PAGE followed by western blotting. Total protein was used as a loading control. A PVDF (Polyvinylidene difluoride) membrane was subjected to Lambda phosphatase treatment according to the manufacturer's instructions (New England BioLabs, Inc.) and immunoblotted again. For semiquantitative analysis, Sarkosyl-insoluble, SDS-soluble fractions from normal and AD brain tissues were subjected to western blotting with recombinant Tau (0N4R) or recombinant MAP2c as the standard. Because phosphorylation can affect the immunoreactivity of antibodies, the membranes were treated with phosphatase and then immunoblotted with the anti-Tau (Tau5) and anti-MAP2 (MAP2-#39 and #41) antibodies.

Immunofluorescence staining

Paraffin-embedded sections (#8097 and #8308) from late-onset AD brains were deparaffinized and pretreated by autoclaving at 120°C for 7 minutes and then with formic acid for 4 minutes. After pretreatment, the sections were incubated with 10% goat serum and then with the primary antibodies. Bound antibodies were visualized with Alexa Fluor 488- or Alexa Fluor 568-conjugated anti-mouse or anti-rabbit IgG antibodies (Invitrogen) and imaged by confocal laser-scanning microscopy (LSM700, Carl Zeiss). The representative results of #8097 are shown.

In vitro aggregation assay

Tau cDNA in the pRK172 vector was a generous gift from Dr. M. Goedert. MAP2c cDNAs were amplified and cloned into *Eco*RI- and *Nde*I-digested sites of the pRK172 vector. Purification

of recombinant proteins (Tau 0N4R, Tau 0N3R, and MAP2c) and heparin-induced aggregation were performed according to a previous procedure with some modifications [26]. Briefly, supernatants of *Escherichia coli*-expressed recombinant proteins from BL21(DE3) were applied to a phosphocellulose column and eluted by a gradient of 0.1 M–0.3 M NaCl. The Tau- and MAP2c-containing fractions were purified further by ammonium sulfate precipitation, and the pellets were dissolved in the homogenization buffer containing 0.5 M NaCl and 2% 2-mercaptoethanol. The solution was heated at 100°C for 5 minutes, and the pellet was removed by centrifugation. The resultant supernatant was fractioned by reverse-phase HPLC. For *in vitro* aggregation, 60 μg/ml of heparin was mixed with 10 μM recombinant proteins, 100 mM NaCl, 10 μM thioflavine-T (ThT), and 10 mM HEPES (pH 7.4). The time-dependent changes in ThT fluorescence were measured at 465±35 nm (excitation) and 535±25 nm (emission) for 7 days. After the 7-day incubation, the mixtures were adjusted to 1% Sarkosyl, incubated for 30 minutes at 4°C, and centrifuged at 120,000× *g* for 15 minutes. The obtained supernatants and pellets (Sarkosyl-soluble and insoluble fractions, respectively) were subjected to SDS-PAGE followed by Coomassie brilliant blue staining.

Antibodies

Site-specific polyclonal antibodies against the carboxyl terminus of MAP2 were raised using KLH-conjugated synthetic peptides (CGGGTPKSAILVPSEK (MAP2-#39), CGGGRVKIESVKL (MAP2-#40), and CGGGITQSPGRSSVAS (MAP2-#41)), which were administered to rabbits via hypodermic injection. We used ELISA to confirm that the raised antisera were specific for recombinant MAP2c and had no cross-reactivity with recombinant Tau. To avoid cross-reactivity with Tau completely, the antisera were passed through Tau-affinity columns in which recombinant Tau was conjugated to the NHS-activated Sepharose 4 Fast Flow (GE Healthcare). These antibodies were then affinity-purified with each corresponding antigen peptide conjugated to the activated thiol Sepharose 4B (GE Healthcare). Purified MAP2 antibodies had no cross-reactivity with Tau detected by western blotting using a gradient dilution of recombinant MAP2c and Tau (Figure S2). Other antibodies that were used are as follows. UNC-119N was raised against a synthetic peptide conjugated to KLH (QQSIAPGSATFPSQMPRGGC). MAP2N (anti-pan-MAP2) was raised against the MAP2 amino-terminal 1–150 amino acids. The antibodies were affinity-purified with the antigenic protein conjugated to activate thiol Sepharose 4B. HM2 (anti-MAP2, Sigma-Aldrich, St. Louis, MO), anti-phospho-MAP2 (Thr1620/1623, Cell Signaling), DM1A (anti-alpha-tubulin, Sigma-Aldrich), HT7 (anti-human Tau, Innogenetics. Zwijndrecht, Belgium), AT8 (anti-phosphoSer-202 and phosphoThr-205 of Tau, Innogenetics), AT100 (anti-phosphoThr-212 and phosphoSer-214 of Tau, Innogenetics), Tau5 (Abnova Corporation), PHF1 (anti-phospho-Ser-396 and 404 of Tau, a generous gift from Dr. Davies), and pool 2 (anti-pan-Tau, a generous gift from Dr. Mori) were also used.

Western blotting

Western blotting was performed as described previously [25]. Briefly, samples were applied to 10% SDS-PAGE and transferred to a PVDF membrane. Bound antibodies were detected by enhanced chemiluminescence (GE Healthcare) or Immunostar LD (Wako Pure Chemical Industries, Ltd., Japan) and imaged using an LAS4000 system (FUJIFILM).

Statistical analysis

The data are expressed as the mean±SEM and were tested by one-way ANOVA followed by Bonferroni–Dunn *post hoc* test if not mentioned. The significance level is 5%.

Results

Neuronal dysfunction is induced by the carboxyl-terminal of Tau

To identify which region is responsible for Tau neurotoxicity, we developed worm models that expressed full-length 0N4R or 0N3R (the four-repeat 383-residue isoform and three-repeat 352-residue isoform of human Tau, respectively), 0N (corresponding to residues 1–192 of 0N4R Tau), and 4R or 3R (corresponding to the residue of 193– the carboxyl terminus of 0N4R and 0N3R Tau, respectively) driven under the pan-neuronal *unc-119* promoter (Figure 1) [19].

We first quantified the exogenously expressed proteins in each line (Figures 2A and 2B). There were two independent lines expressing high and low levels of 0N4R Tau. The levels of Tau were 3.5-fold higher in the high-expression line (tmIs390) than in the low-expression line (tmIs389). The expression levels of 0N3R Tau were nonsignificantly lower in tmIs252 than those of 0N4R Tau in tmIs390. Four R and 3R fragments containing MTBDs tend to form high-molecular-mass bands observed above the lower-molecular-mass bands on SDS-PAGE (Figure 2A). The density of total bands, including the high-molecular-mass and the low-molecular-mass bands were quantified together. The expression of Tau fragments did not differ between 4R (tmIs712), 3R (tmIs709), and 0N (tmIs711).

The percentage of the Unc population in each line was quantified as described in the Materials and methods section. High expression of 0N4R Tau led to severe Unc [75.7±5.9%, $P<0.0001$ versus the mock (tmIs388; the empty vector-transgenic worm line with the expression of UNC-119 peptide tag, 5±5%)] in the worms, but its low expression did not lead to significant abnormalities (5.7±2.3%, $P=0.91$ versus mock). 0N3R Tau had lower toxicity than 0N4R Tau at a similar expression level (Figure 2C). To identify the region responsible for Tau-induced neuronal dysfunction, we compared the Unc populations of 4R, 3R, and 0N Tau fragment-expressing worms. As shown in Figure 2C, 4R fragment-expressing worms exhibited the highest percentage with behavioral abnormality (98.3±1.7%, $P<0.0001$ versus mock). Three R fragment-expressing worms showed a fourfold increase in the percentage expressing the Unc phenotype compared with the mock line, but this increase was not significant (20±5.8% versus 5±5%, $P=0.06$). The expression levels of 4R and 3R fragments were similar to those of the 0N4R/low line and 0N3R Tau, and the fragmentation of Tau may enhance its toxicity to neurons. In sharp contrast to MTBD-containing fragments, 0N Tau fragment-expressing worms showed no abnormality. Thus, we concluded that the carboxyl-terminal region of Tau containing MTBDs is essential for its neurotoxicity.

To examine whether over-expression of exogenous proteins cause neuronal dysfunction, GFP was expressed at a level more than threefold higher than that of Tau, but no neuronal dysfunction was observed. In addition to GFP, we also expressed GSK-3beta, Hsp70 or DsRed, any of which did not induce the Unc phenotype observed in the 0N4R/high and 4R fragment-expressing worms (data not shown). These results suggested that in the *C. elegans* system, the Unc phenotype could be induced only by the specific amino-acid sequences other than over-expression itself.

Neuronal dysfunction is also induced by the carboxyl-terminal of MAP2.

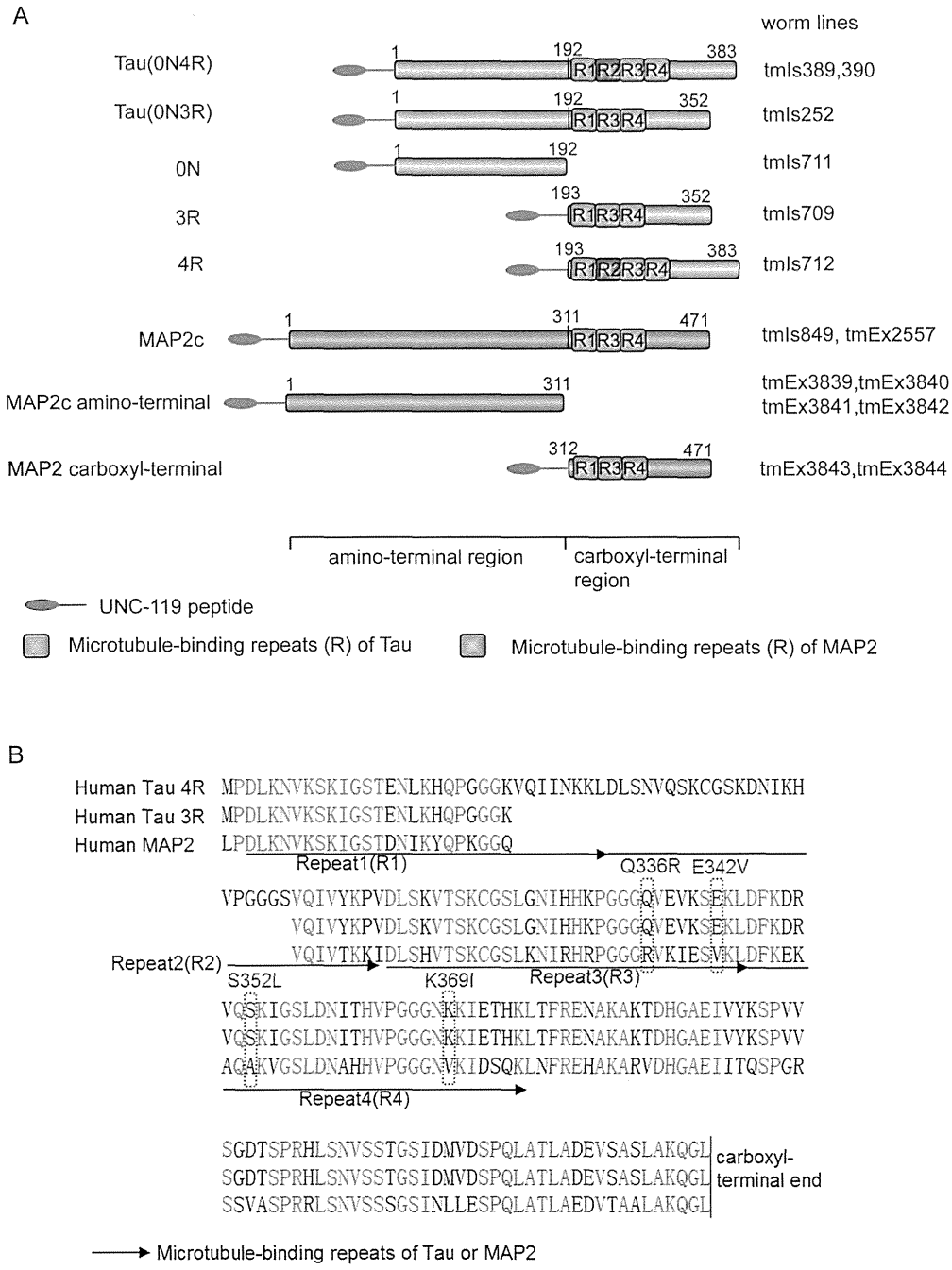

Figure 1. Schematic representation of Tau and MAP2 expressed pan-neuronally in transgenic *C. elegans*. (**A**) Diagrams of expressed proteins, full-length Tau (0N4R and 0N3R), Tau fragments (0N, 3R, and 4R), MAP2c, and MAP2c fragments (MAP2c amino-terminal and carboxyl-terminal) are shown. The Tau and MAP2c microtubule-binding domains (MTBDs) are depicted by blue and purple boxes, respectively. A 23-residue peptide in the UNC-119 amino-terminal assists proper expression and was used as the expression tag linked to the amino-terminus of Tau or MAP2. The numbers written above are the positions of the amino acids. (**B**) Comparison of the carboxyl-terminal amino acid sequences of Tau and MAP2. Identical amino acids are shown in red, and different amino acids are shown in black. Two perfect FTDP-17 mutations, Q336R and E342V, and two imperfect mutations, S325A (S325L in FTDP-17) and K369V (K369I in FTDP-17), that locate within the MAP2 MTBD are indicated.
doi:10.1371/journal.pone.0089796.g001

Because the 160-residue carboxyl-terminal of MAP2, which contains MTBDs, is highly homologous to that of Tau (see Figure 1B), we asked whether neurotoxicity could also be elicited by MAP2. The low-molecular-mass isoform MAP2c shares its entire sequence with the high-molecular-mass MAP2 isoform and is similar in size to Tau. MAP2c and its fragments-transgenic (Tg) worms were developed using the identical pan-neuronal-expressing system under the *unc-119* promoter, as described above (Figure 1A).

As shown in Figures 3A and 3B, MAP2c was expressed at lower levels than was Tau in the 0N4R/high line, although this difference was not significant (3.4±0.5-fold versus 1.6±0.7-fold,

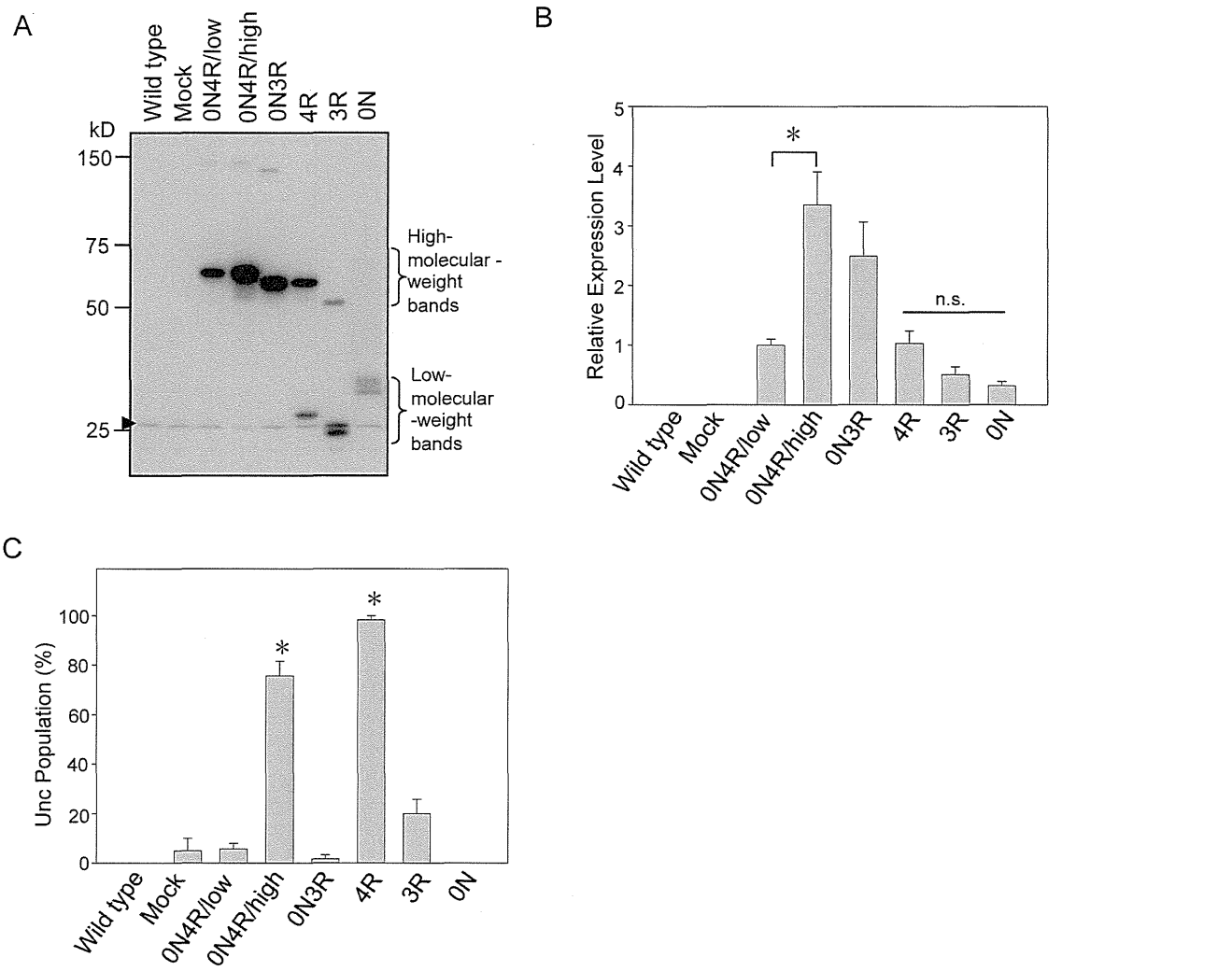

Figure 2. Neuronal dysfunction is induced by the carboxyl-terminal of Tau. (**A**) Representative western blots showing the expressed full-length Tau (0N4R and 0N3R) and its fragments (0N, 3R, and 4R) in transgenic worms. Mock indicates the empty vector-transgenic worm line. Total lysates of the indicated 10 worms were subjected to western blotting using the UNC-119N antibody. The arrowhead indicates endogenous UNC-119. (**B**) The expression of each construct is presented as the relative abundance compared with the 0N4R/low-expressing worm (0N4R/low). n.s. indicates not significant. (**C**) Neurotoxicity was examined in each transgenic worm line. Data indicate the percentage of each worm line that showed uncoordinated movement (Unc). Note that the carboxyl-terminal fragment in 4R-Tg worms had a significantly higher percentage showing the Unc phenotype. 3R-Tg worms showed only a limited degree of Unc, whereas no Unc was observed in 0N-Tg worms. All data are presented as the mean±SEM from three independent experiments. Data were tested by one-way ANOVA followed by the Bonferroni–Dunn *post hoc* test. Asterisks indicate significance versus mock ($P<0.005$, significance level is 5%).
doi:10.1371/journal.pone.0089796.g002

$P = 0.008$). The percentage of MAP2c-expressing worms showing the Unc phenotype was similar to that of the 0N4R/high line (67.5±13.6% versus 75.7±5.9%) and both were significantly higher than that of the mock line (Figure 3C), suggesting that MAP2c induces neuronal dysfunction in *C. elegans*. To indentify the region responsible for MAP2c-induced neuronal dysfunction, we compared the Unc phenotype populations of MAP2c amino-terminal, carboxyl-terminal and full-length-Tg worm lines. As shown in Figure 3D, MAP2 carboxyl-terminal fragments-Tg lines as well as the full-length-Tg line showed high percentage of Unc phenotype. In contrast, MAP2c amino-terminal fragments expressing worms showed less behavioral abnormalities. These results indicate that the carboxyl-terminal region of MAP2 is responsible for its neurotoxicity.

Tau and MAP2 are phosphorylated and do not bind to microtubules in Tg worms

Hyperphosphorylation, which dissociates Tau from microtubules, is a characteristic sign of the AD brain [27,28]. To examine the phosphorylation and microtubule-binding activity of exogenous MAPs in worm neurons, Tau and MAP2 were purified from transgenic worms and subjected to phosphatase treatment, as described in the Materials and methods section. The phosphatase treatment caused significant mobility shifts of Tau and MAP2 on SDS-PAGE, suggesting that both molecules were highly phosphorylated in the worm (Figure 4A). In addition, Tau (both 0N3R and 0N4R) or MAP2, which were expressed in Tg worms, were recognized respectively by anti-phospho-Tau antibodies (AT8 and AT100) or anti-phospho-MAP2 (Thr1620/1623) antibody (data not shown).

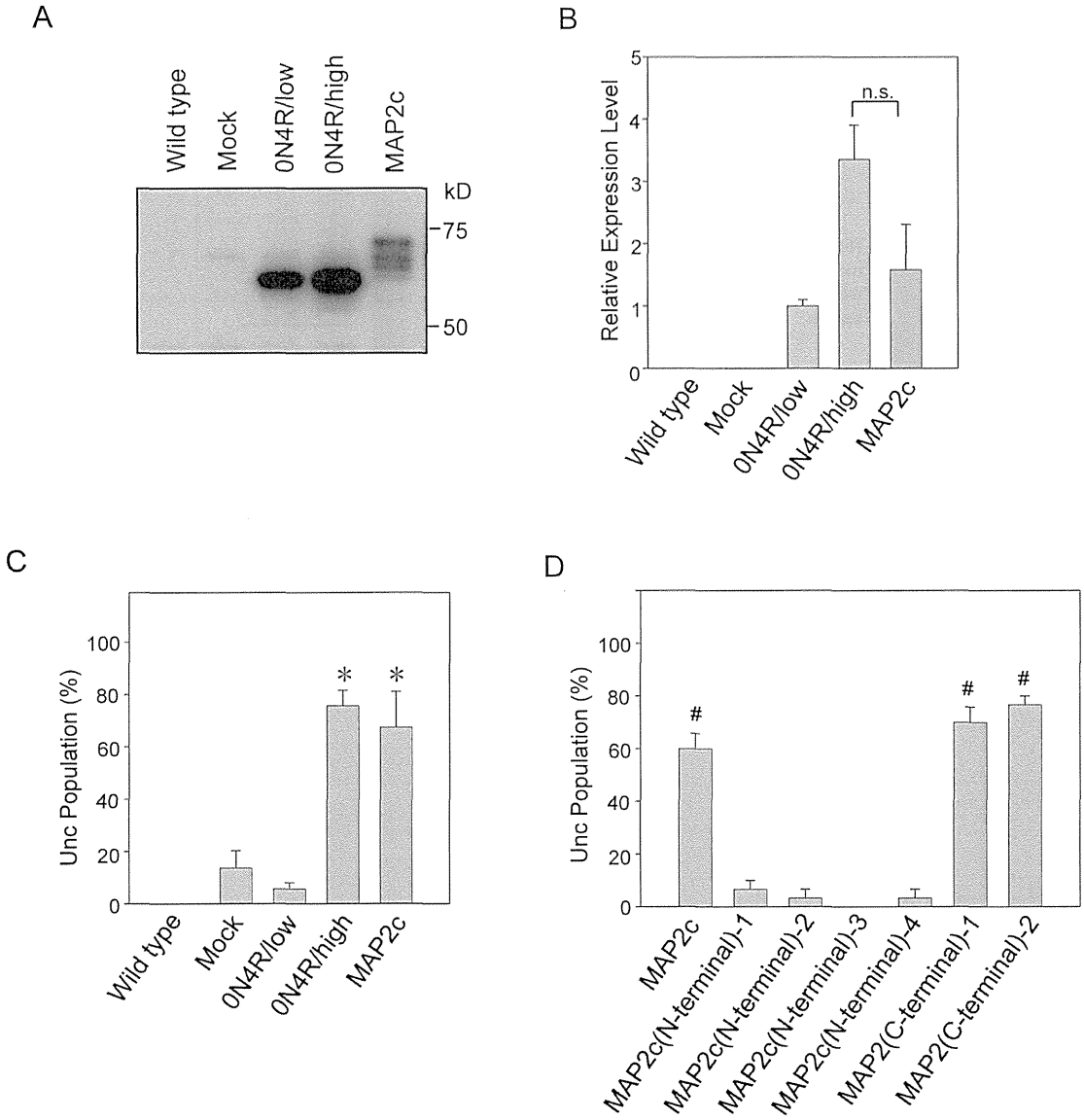

Figure 3. Toxicity of both Tau and MAP2 in worm neurons. (**A**) Representative western blot showing the expression of Tau and MAP2c in transgenic *C. elegans*, as probed with UNC-119N antibody. (**B**) The expression of each construct is presented as the relative abundance compared with the 0N4R/low-expressing line (0N4R/low). No significant difference was observed between the MAP2c and 0N4R/high lines. (**C**) Neuronal dysfunction is induced by MAP2c. Both MAP2c- and Tau 0N4R/high-expressing worms show a significantly higher percentage of worms with the Unc phenotype compared with the mock, indicating that MAP2c was as neurotoxic as Tau. (**D**) The carboxyl-terminal domain of MAP2 is responsible for its neurotoxicity. Unc analysis was performed using the MAP2c full-length (tmEx2557), MAP2c amino(N)-terminal (1 to 4 corresponded to tmEx3839,3840,3841 and 3842, respectively) and MAP2 carboxyl(C)-terminal (1 and 2 corresponded to tmEx3843 and 3844, respectively) Tg lines. The data are expressed as the mean±SEM from at least three independent experiments and were tested by one-way ANOVA followed by the Bonferroni–Dunn *post hoc* test. Asterisks indicate significance versus mock ($P<0.005$, significance level is 5%). # indicate significance versus MAP2c amino-terminal Tg lines ($P<0.005$, significance level is 5%).
doi:10.1371/journal.pone.0089796.g003

Tau and MAP2-Tg worms were subjected to the microtubule-binding assay. After centrifugation under the conditions in which microtubules were stabilized in the buffer containing taxol and GTP, both Tau and MAP2 purified from Tg worms were recovered in the microtubule-unbound fraction in the supernatant but not in the precipitate, suggesting that they were not bound to microtubules because of abnormal hyperphosphorylation (Figure 4B). As described in the previous study, despite PHF-tau and fetal tau are hyperphosphorylated and share several phosphorylated epitopes, fetal tau can bind to microtubules, but PHF-tau loses the function of microtubules binding [27]. Because Tau and MAP2 were not bound to microtubules in the transgenic worms, the present data suggested that both Tau and MAP2 took abnormal forms in the transgenic worm neurons. The liberation of Tau and MAP2 from microtubule may be necessary for the gain of toxic function. Notably, the solubility of both Tau and MAP2 suggested that their neurotoxicity is mediated through a TritonX-100 soluble-form-dependent mechanism in this *C. elegans* system (Figure 4B).

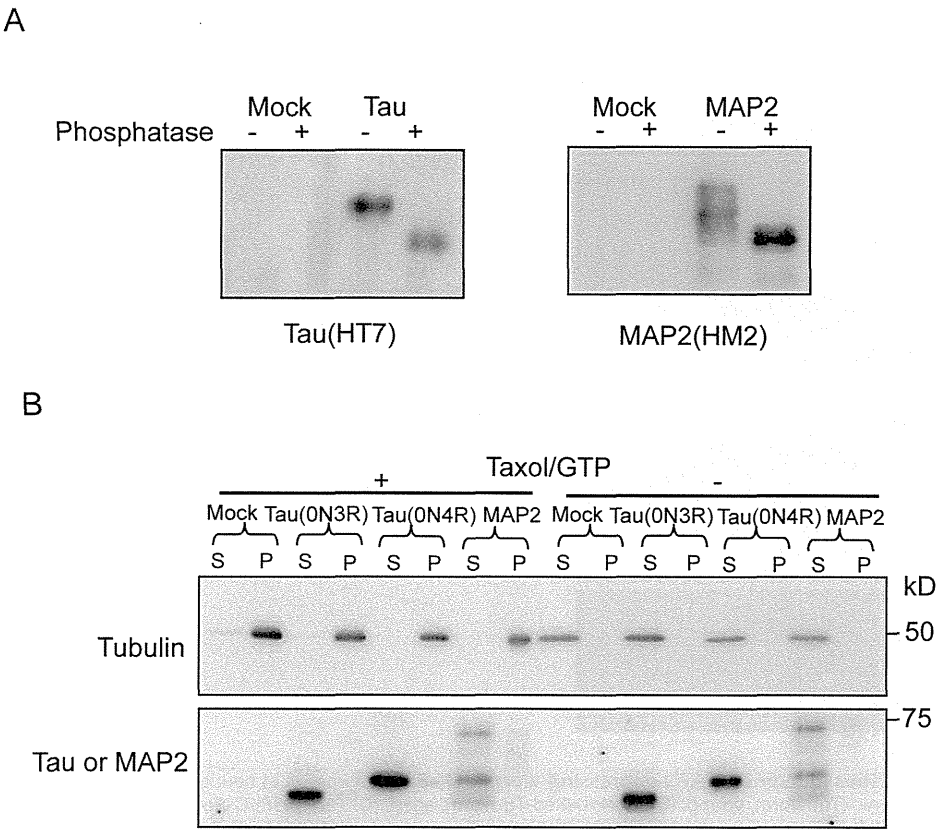

Figure 4. Biochemical characterizations of MAP2c and Tau expressed in transgenic *C. elegans*. (**A**) Both MAP2c and Tau were highly phosphorylated in worm neurons. MAP2c and Tau (0N4R) were purified from the corresponding transgenic worms (MAP2c from tmIs849; 0N4R from tmIs390). Purified proteins were treated with or without phosphatase and subjected to western blotting using the HT7 (anti-human Tau monoclonal) and HM2 (anti-MAP2 monoclonal). (**B**) MAP2c and Tau did not bind to microtubules. The microtubules prepared were stabilized with taxol and GTP, and fractionated into the pellet (P) and supernatant (S). Both MAP2 and Tau remained in the supernatant (S). DM1A (anti-α-tubulin) and anti-UNC-119N (Tau and MAP2c) antibodies were used.
doi:10.1371/journal.pone.0089796.g004

Neuritic abnormalities in Tau and MAP2-Tg worms are age dependent

The expression of Tau or MAP2 in neurons induced significant neuronal dysfunction in worms. We hypothesized that this neuronal dysfunction would correlate with morphological abnormalities in these Tg worms. To address this issue, DsRed, a red fluorescent protein, was expressed under a pan-neuronal *unc-119* promoter to visualize living neurons. DsRed-expressing worms were crossed with mock, Tau (0N3R and 0N4R), and MAP2c-Tg worms. Mock/DsRed-Tg (mock line and DsRed double-Tg) worms had relatively straight neurites, which are considered normal (Figure 5A). By contrast, Tau(0N4R)/DsRed-Tg (0N4R and DsRed double-Tg) and MAP2/DsRed-Tg (MAP2c and DsRed double-Tg) worms exhibited obviously abnormal neurites: many kinks were observed along the neurites, which fluoresced red (Figures 5E–5H). Tau (0N3R)-Tg line showed abnormal morphologies to some extent, but not significantly different from the mock line (Figure5). The number of kinks increased from a few per 100 μm in young worms (4–5 days) to several per 100 μm in aged worms (10–11 days), indicating an age-dependent progression in the appearance of these neuritic abnormalities (Figure 5F). To explore whether Tau(0N4R) or MAP2 was expressed in these abnormal neurites, paraffin sections of mock/DsRed-Tg, Tau(0N4R)/DsRed-Tg, and MAP2/DsRed-Tg worms were prepared. Tau and MAP2 were labeled with anti-Tau (pool 2) and anti-MAP2 (anti-MAP2N) antibodies, respectively. Tau and MAP2 were expressed in abnormal neurites having kinks (Figure S1), indicating that MAP2 and Tau induced similar neuronal abnormalities. We note that the distinct subcellular localization of Tau or MAP2 was not observed in the Tg worms.

MAP2 is not involved in the evolution of NFTs in the AD brain

Next, we examined the contributions of MAP2 and Tau to NFT formation in human AD brains. Following NFT formation, the amino-terminal half of deposited Tau is gradually removed and processed by unknown proteases or spontaneous cleavage through cyclic succinimidyl intermediates, and finally, the residual portion containing MTBDs is left at the PHF core [29,30]. Thus, only antibodies against the MTBDs or their periphery can detect a full range of old to newly deposited Tau [25]. Because the amino-terminal region of MAP2 is much longer than that of Tau expressed in the adult brain, only antibodies against the MTBDs of MAP2 can resolve precisely whether MAP2 is deposited in NFTs.

We found that it was very difficult to distinguish MAP2 from Tau using the carboxyl-terminal antibodies because of high homology in the amino acid sequences between the two molecules (see Figure 1). The commercially available anti-MAP2 antibodies whose epitopes are near the MTBDs easily cross-reacted with Tau

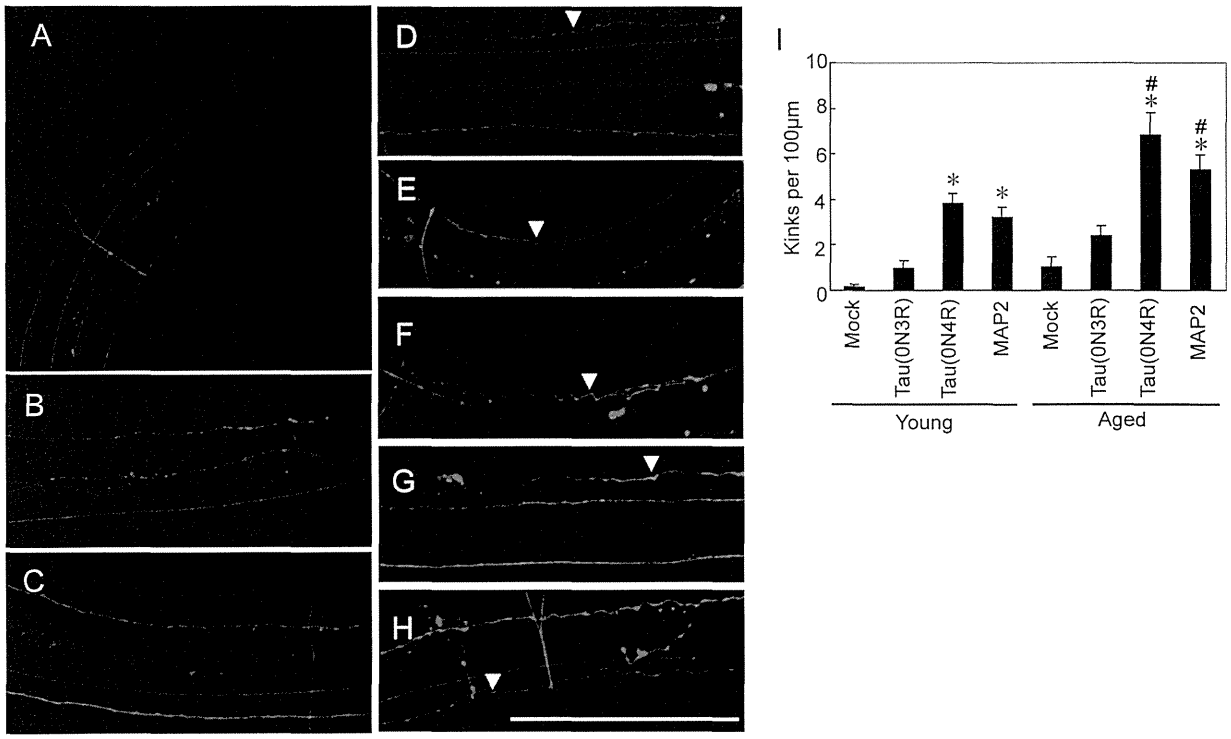

Figure 5. Age-dependent neuritic abnormalities in Tau- or MAP2-expressing worms. (**A–E**) CLSM images of neurites in the posterior part of the worm are shown. (**A**) Mock/DsRed-transgenic (Tg) worm, young. (**B**) Mock/DsRed-Tg worm, aged. (**C**) Tau(0N3R)/DsRed-Tg worm, young. (**D**) Tau(0N3R)/DsRed-Tg worm, aged. (**E**) Tau(0N4R)/DsRed-Tg worm, young. (**F**) Tau(0N4R)/DsRed-Tg worm, aged. (**G**) MAP2/DsRed-Tg worm, young. (**H**) MAP2/DsRed-Tg worm, aged. The scale bar is 100 μm. (**I**) Numbers of abnormal kinks (arrows) per 100 μm neurite. "Young" indicates 4–5 days after hatching, and "aged" indicates 10–11 days. The data are expressed as the mean±SEM. Asterisks indicate significant differences versus mock in each age group (one-way ANOVA followed by Bonferroni–Dunn *post hoc* test). # indicates a significant difference in the young versus aged group in the same line ($P<0.05$, Student's t-test). n = 21 to 23.
doi:10.1371/journal.pone.0089796.g005

(data not shown). Thus, we raised three new independent site-specific anti-MAP2 polyclonal antibodies with epitopes that localize to the carboxyl-terminal sequence, either in or near the MTBDs (Figure 6A). Purified anti-MAP2 antibodies did not cross-react with Tau (Figure S2). Several previous trials tried to investigate whether MAP2 is a component of NFTs by using conventional immunochemical approaches, but the results were conflicting [31–34]. The confusion may have been caused by the relatively low specificities of the antibodies used [35]. As far as we know, this is the first study of the involvement of the carboxyl-terminal region of MAP2 in NFT formation determined using well-characterized antibodies that showed no cross-reaction with Tau. This distinguishes our immunostaining study from the previous works.

Because acquisition of Sarkosyl insolubility is a significant characteristic of deposited Tau in tauopathies [36,37], we first examined the Sarkosyl insolubility of MAP2 in the brains of AD patients and normal controls (Table S1). Brain tissues were homogenized sequentially with TS buffer containing Triton X-100, Sarkosyl, or SDS. The Sarkosyl-insoluble, SDS-soluble fractions were immunoblotted with anti-MAP2 and anti-Tau antibodies. As expected, anti-Tau antibodies showed a characteristic smear staining in the fractions prepared from AD brains compared with those from normal brains. However, none of the three site-specific MAP2 antibodies (MAP2-#39, #40, and #41) showed any increase in smear staining in AD samples compared with normal brains (MAP2-#39 and #40 are not shown, Figure 6B). We semiquantified the amounts of Tau and MAP2 in the Sarkosyl-insoluble, SDS-soluble fractions from AD brains and found that the amount of MAP2 in this fraction was far less than that of Tau (Figure S3).

We next examined the involvement of the carboxyl-terminal epitopes of Tau and MAP2 in NFT formation by immunohistochemical staining of paraffin-embedded sections from AD brain. As shown in Figure 6C, NFTs and neuropil threads (NTs) were labeled intensely with PHF1 antibody but not with MAP2-#41(MAP2-#39 and #40 showed similar results, data not shown.), which reacts with the epitope corresponding to that of PHF1 (see Figure 6A). The phosphatase treatment of the section before staining did not change the results. (data not shown). Double staining with Tau and MAP2 carboxyl-terminal antibodies distinguishes three types of neurons in AD brain: Tau-positive-only, MAP2-positive-only, and Tau and MAP2 double-positive neurons. Notably, even in the double-positive neurons, no co-localization of Tau and MAP2 was observed (Figure 6C). Regardless of the brain area examined, of the total number of Tau-positive neurons, about 30–40% were MAP2-positive, suggesting that MAP2 is lost during progression of NFT formation (Figure 6D). Thus, despite the high degree of homology between the carboxyl-terminal sequences of MAP2 and Tau (see Figure 1), they have differential fates the course of in NFT formation; that is, MAP2 does not deposit aggressively like Tau and is lost from NFT-forming cells in the AD brain.

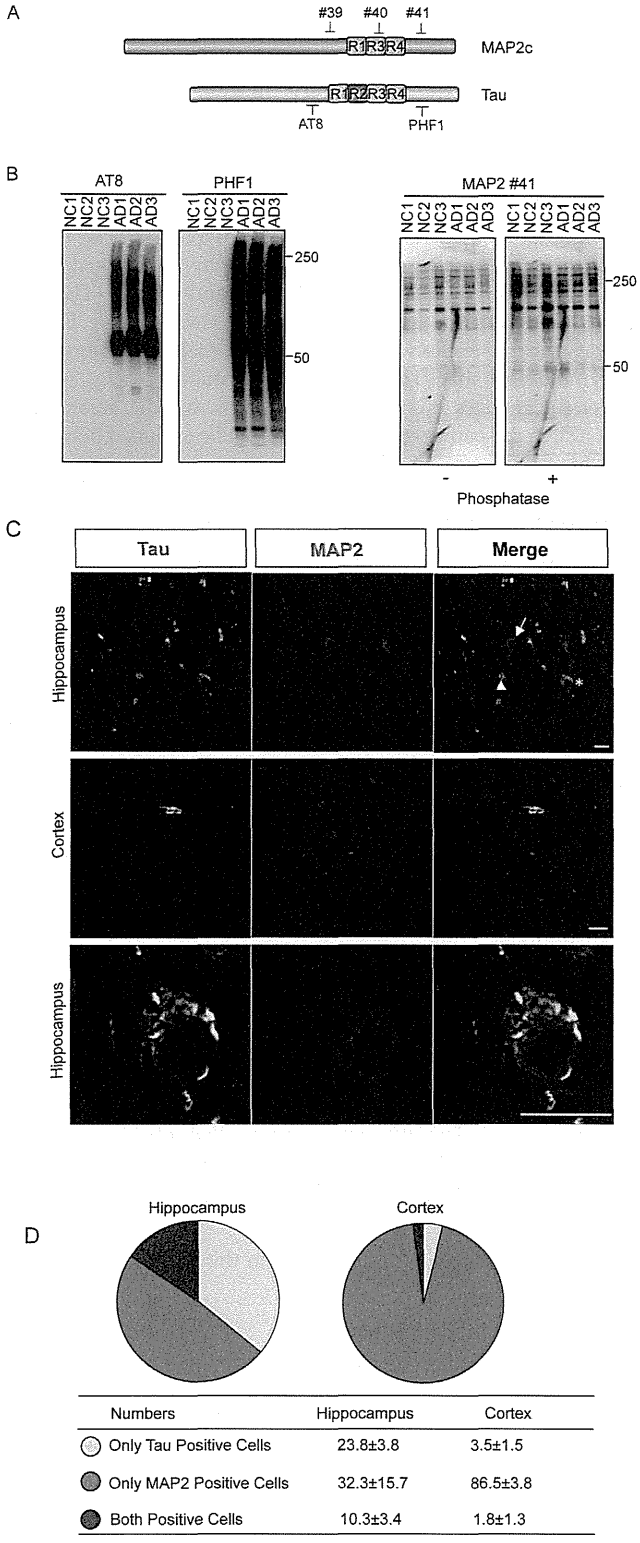

Numbers	Hippocampus	Cortex
Only Tau Positive Cells	23.8±3.8	3.5±1.5
Only MAP2 Positive Cells	32.3±15.7	86.5±3.8
Both Positive Cells	10.3±3.4	1.8±1.3

Figure 6. MAP2 is not involved in the growth process of NFTs in the AD brain. (**A**) Diagram of three site-specific anti-MAP2 antibodies and anti-Tau antibodies. (**B**) Human temporal cortex tissues from three AD patients and three normal controls were homogenized sequentially in detergent-containing buffers. Sarkosyl-insoluble, SDS-soluble fractions were prepared and subjected to SDS-PAGE followed by western blotting using anti-Tau antibodies (AT8 and PHF1) and three newly raised site-specific anti-MAP2 antibodies (MAP2-#39 and #40 are not shown). Total protein was used as the loading control. The staining intensity of Tau was increased markedly in the Sarkosyl-insoluble, SDS-soluble fractions from AD brains compared with normal brains. By contrast, the MAP2 antibodies failed to detect any increased patterns in AD brains compared with normal brains. Phosphatase treatment was performed to avoid effects from MAP2 phosphorylation. NC, normal brains; AD, Alzheimer's disease brains. Information about the cases is provided in Table S1. (**C**) Double immunofluorescence staining of the homologous carboxyl-terminal sequences of Tau and MAP2 in the AD brain. AD brain paraffin-embedded sections were double-labeled by anti-Tau antibody (PHF1) and anti-MAP2 antibody (MAP2-#41). Tau but not MAP2 localized in NFTs as well as in NTs. Representative Tau-positive-only neurons (arrowhead), MAP2-positive-only neurons (arrow) and Tau/MAP2-double-positive neurons (star) are indicated. Scale bars = 25 μm. (**D**) Average number of the three neuron types was counted per 640 μm^2. The data are presented as the mean±SD.
doi:10.1371/journal.pone.0089796.g006

Tau but not MAP2c forms ThT-positive, insoluble aggregates in the presence of heparin

We next asked what caused the differential fates of the homologous carboxyl-terminal sequences of Tau and MAP2 in NFT formation. To investigate this dissociation, we used purified recombinant proteins and compared the aggregation potential of Tau and MAP2 in the presence of heparin *in vitro*. ThT fluorescence was used to monitor the aggregation of Tau or MAP2c [26]. As shown in Figure 7A, Tau and MAP2c showed significantly different aggregation profiles. The ThT fluorescence level of Tau remained constant in the first 4 hours and then increased sharply to reach a plateau at about 24 hours. By contrast, the ThT fluorescence level of MAP2c increased more rapidly in the first 4 hours but did not continue and remained constant after 4 hours, suggesting that MAP2c was unable to form large aggregates to the same extent as Tau. This characteristic was not affected by the different amino-terminal halves (data not shown). After incubation for 1 week, the Sarkosyl solubility of the fractions was examined. More Tau than MAP2c was found in the Sarkosyl-insoluble fraction, suggesting that more stable aggregates were formed by Tau than by MAP2c, an observation that is consistent with the results of ThT fluorescence (Figure 7). We acknowledge that the conditions are more complex *in vivo*, but the intrinsic difficulty of MAP2 accumulation might explain its loss from the growing process of NFTs.

Discussion

In this study, MAP2 or Tau from worm neurons was found to be soluble, strongly suggesting that the neurotoxicity induced by either protein was independent of detergent-insoluble aggregates (Figure 4). This result is consistent with our previous studies suggesting that abnormalities of neurons can be induced by Tau through a nonaggregation mechanism [18]. Santacruz et al. reported NFT-independent neurotoxicity of Tau in a transgenic mice model [38]. This view is also strengthened by a previous quantitative study, which showed that the number of lost neurons was several times higher than NFT-bearing neurons in the AD cortex [39]. These observations suggest that an inclusion-independent mechanism is involved in neuronal loss and thus in the pathogenesis of AD. Here, we found using *C. elegans* that MAP2 and Tau showed similar neurotoxicity in the absence of detergent-insoluble aggregates. Thus, one should not exclude the potential pathological role of MAP2 in the pathogenesis of AD and tauopathies simply because MAP2 barely accumulates in NFTs or in neurons. The highly homologous sequences shared by Tau and MAP2 that exhibit similar neurotoxicity have different fates in the process of NFT formation in the AD brain, as shown by the newly

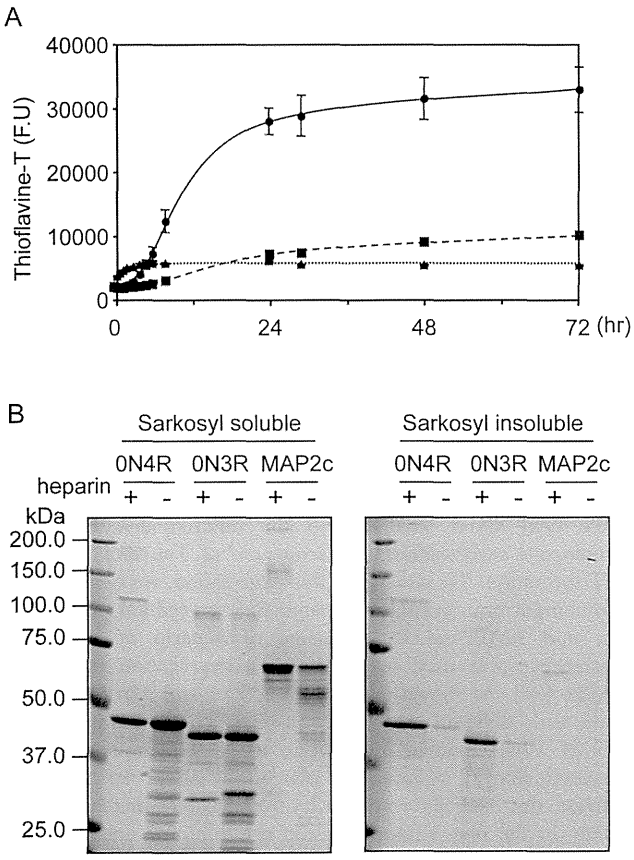

Figure 7. Tau but not MAP2c forms ThT-positive insoluble aggregates induced by heparin. (**A**) The ThT fluorescence of Tau 0N4R isoform (circles), Tau 0N3R isoform (squares), and MAP2c (triangles) aggregates were measured at the times indicated. (**B**) After the 7-day incubation, the amount of Sarkosyl-insoluble proteins in the indicated samples was analyzed by SDS-PAGE followed by Coomassie brilliant blue staining.
doi:10.1371/journal.pone.0089796.g007

raised MAP2 carboxyl-terminal site-specific antibodies used in this study.

The present results indicated that four-repeat Tau is significantly neurotoxic but three-repeat Tau is not (Figure 2). Because MAP2 is predominantly in the three-repeat form in mammalian neurons, the question arises why three-repeat MAP2 showed significantly greater neurotoxicity than three-repeat Tau. We compared the carboxyl-terminal amino acid sequences, as shown in Figure 1B, which are highly homologous between MAP2 and Tau. Aside from the homologous amino acid sequences, there are some differences in amino acids between Tau and MAP2. It is possible that these distinct amino acids make MAP2 more toxic than three-repeat Tau. The hereditary FTDP-17 form of dementia is caused by mutations in the Tau gene. Previous studies have indicated that these mutations increase Tau pathology through apparently different mechanisms, such as increasing four-repeat Tau isoforms by affecting the splicing pattern or increasing Tau aggregation. Interestingly, two perfect FTDP-17 mutations, Q336R and E342V, and two imperfect mutations, S325A (S325L in FTDP-17) and K369V (K369I in FTDP-17), are observed in MAP2 MTBDs [40–43] (Figure 1B). The presence of FTDP-17 mutations in the MAP2 sequence may increase its neurotoxicity to a greater extent.

The present study raises the possibility of a pathoetiological role of MAP2 in the generation of AD and tauopathies. The regions responsible for both aggregation and toxicity are located in the same carboxyl-terminal portions of Tau and MAP2. Thus far, aggregation has been the focus of research, and therefore Tau has been considered exclusively as a pathogenic molecule. Our present study indicates that Tau and MAP2 exhibit toxicity without forming aggregates in worms. This suggests that the involvement of MAP2 in the pathogenesis of AD cannot be excluded because of the absence of its aggregates.

Supporting Information

Figure S1 Abnormal neurites expressing Tau or MAP2. The paraffin sections of 5-day-old worms (Is388/592, DsRed/mock-transgenic(Tg) worm; Is390/592, DsRed/Tau-Tg worm; Is849/592, DsRed/MAP2-Tg worm) used in Figure 5 were colabeled with anti-DsRed and either pool 2 (anti-Tau) or MAP2N (anti-MAP2). Arrows indicate the normal neurites. Abnormal kinks (arrowheads) are observed in the neurites expressing MAP2 or Tau. Scale bar = 20 μm. n = 6–12.
(TIF)

Figure S2 The three independent site-specific MAP2 antibodies did not cross-react with Tau. Purified recombinant MAP2c and Tau (0N4R) linked with His-tags at the amino-terminals were subjected to western blotting using anti-His tag and anti-MAP2 antibodies (#39, #40, and #41).
(TIF)

Figure S3 Semiquantification of Tau and MAP2 in Sarkosyl-insoluble, SDS-soluble fractions from human autopsy samples from normal and advanced AD brains. Note that standards made of recombinant Tau and MAP2 showed similar staining levels. The amount of Tau was greater than that of MAP2 in the Sarkosyl-insoluble/SDS-soluble fractions from advanced AD brains. NC, normal brain; AD, Alzheimer's disease brain.
(TIF)

Table S1 Information of cases used in this study.
(PDF)

Text S1 Supporting Methods.
(PDF)

Author Contributions

Conceived and designed the experiments: CX TM. Performed the experiments: CX TM S. Yoshimura. Analyzed the data: CX TM. Contributed reagents/materials/analysis tools: CX TM HH S. Yoshina EKN S. Mitani S. Murayama YI. Wrote the paper: CX TM YI.

References

1. Lee VM, Goedert M, Trojanowski JQ (2001) Neurodegenerative tauopathies. Annu Rev Neurosci 24: 1121–59.
2. Mandelkow EM, Mandelkow E (2012) Biochemistry and cell biology of tau protein in neurofibrillary degeneration. Cold Spring Harb Perspect Med 2(7): a006247.
3. Kondo J, Honda T, Mori H, Hamada Y, Miura R, et al. (1988) The carboxyl third of tau is tightly bound to paired helical filaments. Neuron 1: 827–34.
4. Wischik CM, Novak M, Thøgersen HC, Edwards PC, Runswick MJ, et al. (1988) Isolation of a fragment of tau derived from the core of the paired helical filament of Alzheimer disease. Proc. Natl. Acad. Sci. USA 85: 4506–10.
5. Wolfe MS (2009) Tau mutations in neurodegenerative diseases. J Biol Chem. 284(10): 6021–5.

6. Amadoro G, Serafino AL, Barbato C, Ciotti MT, Sacco A, et al. (2004) Role of N-terminal tau domain integrity on the survival of cerebellar granule neurons. Cell Death Differ 11: 217–30.
7. Kanaan NM, Morfini G, Pigino G, LaPointe NE, Andreadis A, et al. (2012) Phosphorylation in the amino terminus of tau prevents inhibition of anterograde axonal transport. Neurobiol Aging 33: 826.e15–30.
8. Park SY, Ferreira A (2005) The generation of a 17 kDa neurotoxic fragment: an alternative mechanism by which tau mediates beta-amyloid-induced neurodegeneration. J Neurosci 25: 5365–75.
9. Hirokawa N, Funakoshi T, Sato-Harada R, Kanai Y (1996) Selective stabilization of tau in axons and microtubule-associated protein 2C in cell bodies and dendrites contributes to polarized localization of cytoskeletal proteins in mature neurons. J Cell Biol 132: 667–79.
10. Kanai Y, Hirokawa N (1995) Sorting mechanisms of tau and MAP2 in neurons: suppressed axonal transit of MAP2 and locally regulated microtubule binding. Neuron 14: 421–32.
11. Dehmelt L, Halpain S (2004) The MAP2/Tau family of microtubule-associated proteins. Genome Biol 6: 204.
12. Harada A, Oguchi K, Okabe S, Kuno J, Terada S, et al. (1994) Altered microtubule organization in small-calibre axons of mice lacking tau protein. Nature 369: 488–91.
13. Teng J, Takei Y, Harada A, Nakata T, Chen J, et al. (2001) Synergistic effects of MAP2 and MAP1B knockout in neuronal migration, dendritic outgrowth, and microtubule organization. J Cell Biol 155: 65–76.
14. Brandt R, Gergou A, Wacker I, Fath T, Hutter H (2009) A Caenorhabditis elegans model of tau hyperphosphorylation: induction of developmental defects by transgenic overexpression of Alzheimer's disease-like modified tau. Neurobiol Aging 30: 22–33.
15. Calahorro F, Ruiz-Rubio M (2011) Caenorhabditis elegans as an experimental tool for the study of complex neurological diseases: Parkinson's disease, Alzheimer's disease and autism spectrum disorder. Invert Neurosci 11: 73–83.
16. Fatouros C, Pir GJ, Biernat J, Koushika SP, Mandelkow E, et al. (2012) Inhibition of tau aggregation in a novel Caenorhabditiselegans model of tauopathy mitigates proteotoxicity. Hum Mol Genet 21: 3587–603.
17. Kraemer BC, Zhang B, Leverenz JB, Thomas JH, Trojanowski JQ, et al. (2003) Neurodegeneration and defective neurotransmission in a Caenorhabditis elegans model of tauopathy. Proc. Natl. Acad. Sci. USA 100: 9980–5.
18. Miyasaka T, Ding Z, Gengyo-Ando K, Oue M, Yamaguchi H, et al. (2005a) Progressive neurodegeneration in C. elegans model of tauopathy. Neurobiol Dis 20: 372–83.
19. Maduro M, Pilgrim D (1995) Identification and cloning of unc-119, a gene expressed in the Caenorhabditis elegans nervous system. Genetics 141:977–88.
20. Brenner S (1974) The genetics of Caenorhabditis elegans. Genetics 77: 71–94.
21. Mello C, Fire A (1995) DNA transformation. Methods Cell Biol 48: 451–82.
22. Mitani S (1995) Genetic regulation of mec-3 gene expression implicated in the specification of the mechanosensory neuron cell types in Caenorhabditis elegans. Dev Growth Diff 37: 551–557.
23. Miyasaka T, Sato S, Tatebayashi Y, Takashima A (2010) Microtubule destruction induces tau liberation and its subsequent phosphorylation. FEBS Lett 584:3227–32.
24. Braak H, Braak E (1991) Neuropathological stageing of Alzheimer-related changes. Acta Neuropathol 82: 239–59.
25. Miyasaka T, Watanabe A, Saito Y, Murayama S, Mann DM, et al. (2005b) Visualization of newly deposited tau in neurofibrillary tangles and neuropil threads. J Neuropathol Exp Neurol 64: 665–74.
26. Maeda S, Sahara N, Saito Y, Murayama M, Yoshiike Y, et al. (2007) Granular tau oligomers as intermediates of tau filaments. Biochemistry. 46:3856–61.
27. Yoshida H., Ihara Y (1993) Tau in paired helical filaments is functionally distinct from fetal tau: assembly incompetence of paired helical filament-tau. J Neurochem 61: 1183–6.
28. Morishima-Kawashima M, Hasegawa M, Takio K, Suzuki M, Yoshida H, et al. (1995) Hyperphosphorylation of tau in PHF. Neurobiol Aging 16: 365–71.
29. Endoh R, Ogawara M, Iwatsubo T, Nakano I, Mori H (1993) Lack of the carboxyl terminal sequence of tau in ghost tangles of Alzheimer's disease. Brain Res 601:164–72.
30. Watanabe A, Takio K, Ihara Y (1999) Deamidation and isoaspartate formation in smeared tau in paired helical filaments.Unusual properties of the microtubule-binding domain of tau. J Biol Chem 274:7368–78.
31. Ashford JW, Soultanian NS, Zhang SX, Geddes JW (1998) Neuropil threads are collinear with MAP2 immunostaining in neuronal dendrites of Alzheimer brain. J Neuropathol Exp Neurol 57: 972–8.
32. Dammerman M, Yen SH, Shafit-Zagardo B (1989) Sequence of a human MAP-2 region sharing epitopes with Alzheimer neurofibrillary tangles. J Neurosci Res 24: 487–95.
33. Kosik KS, Duffy LK, Dowling MM, Abraham C, McCluskey A, et al. (1984) Microtubule-associated protein 2: monoclonal antibodies demonstrate the selective incorporation of certain epitopes into Alzheimer neurofibrillary tangles. Proc Natl Acad Sci USA 81: 7941–5.
34. Rosemblatt M, Fellous A, Mazie JC, Delacourte A, Defossez A (1989) Alzheimer's disease: microtubule-associated proteins 2 (MAP2) are not components of paired helical filaments. FEBS Lett 252: 91–4.
35. Nukina N, Kosik KS, Selkoe DJ (1987) Recognition of Alzheimer paired helical filaments by monoclonal neurofilament antibodies is due to crossreaction with tau protein. Proc. Natl. Acad. Sci. USA 84: 3415–9.
36. Greenberg SG, Davies P (1990) A preparation of Alzheimer paired helical filaments that displays distinct tau proteins by polyacrylamide gel electrophoresis. Proc. Natl. Acad. Sci. USA 87: 5827–5831
37. Lee VM, Balin BJ, Otvos L Jr, Trojanowski JQ (1991) A68: a major subunit of paired helical filaments and derivatized forms of normal Tau. Science 251:675–8.
38. Santacruz K, Lewis J, Spires T, Paulson J, Kotilinek L, et al. (2005) Tau Suppression in a Neurodegenerative Mouse Model Improves Memory Function. Science. 309: 476–481.
39. Gomez-Isla T, Hollister R, West H, Mui S, Growdon JH, et al. (1997) Neuronal loss correlates with but exceeds neurofibrillary tangles in Alzheimer's disease. Ann. Neurol. 41: 17–24.
40. Lippa CF, Zhukareva V, Kawarai T, Uryu K, Shafiq M, et al. (2000) Frontotemporal dementia with novel tau pathology and a Glu342Val tau mutation. Ann Neurol 48: 850–8
41. Neumann M, Schulz-Schaeffer W, Crowther RA, Smith MJ, Spillantini MG, et al. (2001) Pick's disease associated with the novel Tau gene mutation K369I. Ann Neurol 50:503–13.
42. Nicholl DJ, Greenstone MA, Clarke CE, Rizzu P, Crooks D, et al. (2001) An English kindred with a novel recessive tauopathy and respiratory failure. Ann Neurol 54:682–6.
43. Pickering-Brown SM, Baker M, Nonaka T, Ikeda K, Sharma S, et al. (2004) Frontotemporal dementia with Pick-type histology associated with Q336R mutation in the tau gene. Brain 127:1415–26.

Evaluation of *SLC20A2* mutations that cause idiopathic basal ganglia calcification in Japan

Megumi Yamada, MD*
Masaki Tanaka, MD*
Mari Takagi, BA
Seiju Kobayashi, MD, PhD
Yoshiharu Taguchi, MD, PhD
Shutaro Takashima, MD, PhD
Kortaro Tanaka, MD, PhD
Tetsuo Touge, MD, PhD
Hiroyuki Hatsuta, MD
Shigeo Murayama, MD, PhD
Yuichi Hayashi, MD, PhD
Masayuki Kaneko, PhD
Hiroyuki Ishiura, MD, PhD
Jun Mitsui, MD, PhD
Naoki Atsuta, MD, PhD
Gen Sobue, MD, PhD
Nobuyuki Shimozawa, MD, PhD
Takashi Inuzuka, MD, PhD
Shoji Tsuji, MD, PhD
Isao Hozumi, MD, PhD

Correspondence to
Dr. Hozumi:
hozumi@gifu-pu.ac.jp

Supplemental data at
www.neurology.org

ABSTRACT

Objective: To investigate the clinical, genetic, and neuroradiologic presentations of idiopathic basal ganglia calcification (IBGC) in a nationwide study in Japan.

Methods: We documented clinical and neuroimaging data of a total of 69 subjects including 23 subjects from 10 families and 46 subjects in sporadic cases of IBGC in Japan. Mutational analysis of *SLC20A2* was performed.

Results: Six new mutations in *SLC20A2* were found in patients with IBGC: 4 missense mutations, 1 nonsense mutation, and 1 frameshift mutation. Four of them were familial cases and 2 were sporadic cases in our survey. The frequency of families with mutations in *SLC20A2* in Japan was 50%, which was as high as in a previous report on other regions. The clinical features varied widely among the patients with *SLC20A2* mutations. However, 2 distinct families have the same mutation of S637R in *SLC20A2* and they have similar characteristics in the clinical course, symptoms, neurologic findings, and neuroimaging. In our study, all the patients with *SLC20A2* mutations showed calcification. In familial cases, there were symptomatic and asymptomatic patients in the same family.

Conclusion: *SLC20A2* mutations are a major cause of familial IBGC in Japan. The members in the families with the same mutation had similar patterns of calcification in the brain and the affected members showed similar clinical manifestations. *Neurology*® 2014;82:705–712

GLOSSARY

DNTC = diffuse neurofibrillary tangles with calcification; **FIBGC** = familial idiopathic basal ganglia calcification; **IBGC** = idiopathic basal ganglia calcification; **MMSE** = Mini-Mental State Examination; **PDGF** = platelet-derived growth factor; **PDGFRB** = platelet-derived growth factor receptor-β; **Pi** = inorganic phosphate; **PiB** = Pittsburgh compound B; **PiT** = type III sodium-dependent phosphate transporter; **PKC** = paroxysmal kinesigenic choreoathetosis.

Idiopathic basal ganglia calcification (IBGC), also known as Fahr disease, is thought to be a rare neuropsychiatric disorder characterized by symmetrical calcification in the basal ganglia and other brain regions. Clinical manifestations range widely from asymptomatic to variable symptoms including headaches, psychosis, and dementia.[1] The diagnosis of IBGC generally relies on the visualization of bilateral calcification mainly in the basal ganglia by neuroimaging and the absence of metabolic, infectious, toxic, or traumatic causes.[2,3]

The mode of inheritance of familial IBGC (FIBGC) has been thought to be autosomal dominant and, to date, 4 responsible chromosomal regions have been identified, namely 14q (IBGC1), 2q37 (IBGC2), 8p11.21 (IBGC3), and 5q32 (IBGC4).[3–14] The causative gene at the IBGC3 locus was identified as *SLC20A2* encoding type III sodium-dependent phosphate transporter 2 (PiT-2). Screening of a large series of patients with IBGC revealed that mutations in *SLC20A2* are a major cause of FIBGC[10]; moreover, other mutations in *SLC20A2* have recently been reported in China and Brazil.[11–13] The mutations of *PDGFRB* encoding platelet-derived growth factor

*These authors contributed equally to this work.

From the Laboratory of Medical Therapeutics and Molecular Therapeutics (Y.M., M. Takagi, Y.H., M.K., I.H.), Gifu Pharmaceutical University, Gifu; Department of Neurology (M. Tanaka, H. I., J.M., S. Tsuji), The University of Tokyo; Department of Neurology (N.A., G.S.), Nagoya University; Department of Neuropsychiatry (S.K.), Sapporo Medical University, Sapporo; Department of Neurology (Y.Y., S. Takashima, K.T.), Toyama University Hospital, Toyama; Department of Neurology (T.T.), Kagawa University Hospital, Kagawa; Department of Neurology (H.H, S.M.), Tokyo Metropolitan Institute of Gerontology, Tokyo; Department of Neurology and Geriatrics (M.Y., Y.H., T.I.), and Division of Genomic Research, Life Science Research Center (N.S.), Gifu University, Gifu, Japan.

Go to Neurology.org for full disclosures. Funding information and disclosures deemed relevant by the authors, if any, are provided at the end of the article.

(PDGF) receptor-β (PDGFRB) and *PDGFB* have recently been reported to cause calcification in the brain.[14,15]

We have collected clinical information of patients with IBGC in a nationwide survey in Japan. Here, on the basis of a mutational analysis of *SLC20A2*, we aim to establish the molecular epidemiology of IBGC3 and evaluate clinically and genetically *SLC20A2* mutations in Japan.

METHODS Subjects and samples. We collected clinical information on patients with IBGC in a nationwide study. The criteria for the selection of patients in the initial survey were as follows: 1) conspicuous calcification is observed in the basal ganglia and/or dentate nucleus by CT scan; 2) calcification is bilateral and symmetrical; and 3) idiopathic (absence of biochemical abnormalities, and an infectious, toxic, or traumatic cause).[2,3] Neurologists enrolled patients in the survey. They examined the medical charts and performed the neurologic examinations again if necessary. The survey was approved by the Ethics Committee of the Gifu University Graduate School of Medicine. During the survey, some patients were found to have hypoparathyroidism, Aicardi-Goutières syndrome, and Cockayne syndrome, and these patients were excluded. For the genetic study, a total of 69 subjects from 41 hospitals provided written informed consent and were enrolled in the project. Of these patients, 46 came from families with a single affected member, and the other 23 came from 10 families with multiple affected members. We defined the former as sporadic patients and the latter as familial patients. The patients' mean age ± SD was 41.3 ± 23.6 years at registration. The patients comprised 32 males and 37 females.

Standard protocol approvals, registrations, and patient consents. All experiments on human DNA were approved by the Ethics Committees of both Gifu University and the University of Tokyo. After written informed consent was obtained, peripheral blood samples were collected.

Mutational analysis. Genomic DNA was extracted from the whole blood samples. *SLC20A2* analysis was performed by Sanger sequencing of all coding regions, as described in detail in e-Methods and table e-1, A and B, on the *Neurology*® Web site at www.neurology.org. The pathologic potential of the identified variants was predicted using PolyPhen-2 (http://genetics.bwh.harvard.edu/pph/).[16]

RESULTS Mutational analysis. We screened a total of 69 subjects including 23 subjects from 10 families in which multiple affected subjects were observed and 46 subjects in sporadic cases, all of whom were Japanese. Six new mutations in *SLC20A2* were found: 4 missense mutations, 1 nonsense mutation, and 1 frameshift mutation (figure 1). Electropherograms showed the individual heterozygous mutations (figure e-1). None of them were present in an in-house exome sequencing data set (358 Japanese control subjects), dbSNP 137 (www.ncbi.nlm.nih.gov/snp/), or the National Heart, Lung, and Blood Institute "Grand Opportunity" Exome Sequencing Project (ESP6500SI-V2). In silico analysis predicted deleterious consequences, as determined from the residue changes in figures 1 and e-1. When confined to the FIBGC patients, 5 of the 10 families (50.0%) showed mutations in *SLC20A2*. In contrast, 2 of the 46 patients (4.3%) with sporadic IBGC carried mutations in *SLC20A2* in this study.

Clinical manifestations. The clinical manifestations are summarized in table 1. A positive family history of IBGC was present in 5 families. Families 1 and 2 had the same mutation.

Familial cases. ***Case 1 (in family 1).*** The proband in family 1 was a 64-year-old woman who had dysarthria and gait disturbance for 5 years. She showed no dementia. Her neurologic examination revealed dysarthria, small steppage gait, rigidity at bilateral wrist joints, bradykinesia, and a pyramidal sign. Her CT images revealed severe calcification at the bilateral globus pallidus, caudate nuclei, thalamus, subcortical white matter, and dentate nuclei (figure 2C). Her son's CT showed similar brain calcification (figure 2D), although he was clinically asymptomatic. His DNA study revealed the

Figure 1 Schematic representation of causative mutations in SLC20A2 in idiopathic basal ganglia calcification

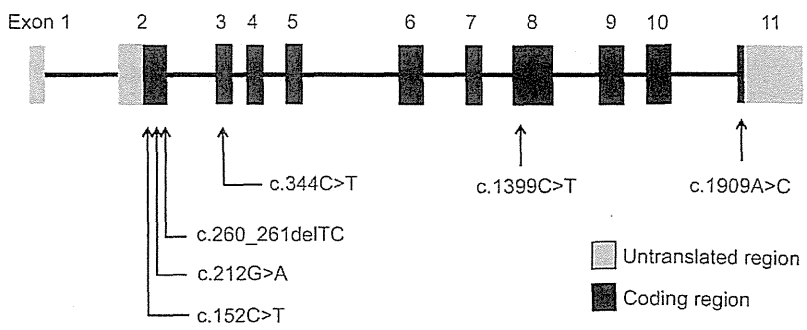

Six new causative mutations in exon 2 (c.152C>T, c.212 G>A, c.260_261delTC), exon 3 (c.344C>T), exon 8 (c.1399C>T), and exon 11 (c.1909A>C) were found in this study.